AD_____

Award Number: DAMD17-94-C-4064

TITLE: Non-Invasive Detection of Axillary Nodes by Contrast Enhanced Magnetic Resonance Imaging

PRINCIPAL INVESTIGATOR: Jason Koutcher, M.D., Ph.D.

CONTRACTING ORGANIZATION: Sloan-Kettering Institute for Cancer Research
New York, New York 10021

REPORT DATE: October 1999

TYPE OF REPORT: Final

PREPARED FOR: U.S. Army Medical Research and Materiel Command
Fort Detrick, Maryland 21702-5012

DISTRIBUTION STATEMENT: Approved for public release
distribution unlimited

The views, opinions and/or findings contained in this report are those of the author(s) and should not be construed as an official Department of the Army position, policy or decision unless so designated by other documentation.

JasonREPORT DOCUMENTATION PAGE

Form Approved
OMB No. 074-0188

Public reporting burden for this collection of information is estimated to average 1 hour per response, including the time for reviewing instructions, searching existing data sources, gathering and maintaining the data needed, and completing and reviewing this collection of information. Send comments regarding this burden estimate or any other aspect of this collection of information, including suggestions for reducing this burden to Washington Headquarters Services, Directorate for Information Operations and Reports, 1215 Jefferson Davis Highway, Suite 1204, Arlington, VA 22202-4302, and to the Office of Management and Budget, Paperwork Reduction Project (0704-0188), Washington, DC 20503

1. AGENCY USE ONLY (Leave blank)	2. REPORT DATE October 1999	3. REPORT TYPE AND DATES COVERED Final (16 Sep 94 - 15 Sep 99)

4. TITLE AND SUBTITLE
Non-Invasive Detection of Axillary Nodes by Contrast Enhanced Magnetic Resonance Imaging

5. FUNDING NUMBERS
DAMD17-94-C-4064

6. AUTHOR(S)
Jason Koutcher, M.D., Ph.D.

7. PERFORMING ORGANIZATION NAME(S) AND ADDRESS(ES)
Sloan-Kettering Institute for Cancer Research
New York, New York 10021

e-mail: koutchej@mskcc.org

8. PERFORMING ORGANIZATION REPORT NUMBER

9. SPONSORING / MONITORING AGENCY NAME(S) AND ADDRESS(ES)

U.S. Army Medical Research and Materiel Command
Fort Detrick, Maryland 21702-5012

10. SPONSORING / MONITORING AGENCY REPORT NUMBER

11. SUPPLEMENTARY NOTES

12a. DISTRIBUTION / AVAILABILITY STATEMENT
Approved for public release
distribution unlimited

12b. DISTRIBUTION CODE

13. ABSTRACT *(Maximum 200 Words)*

Previous studies in murine tumors have shown that the 3 drug combination of PALA + MMPR + 6AN (PMA) [PALA (n-phosphonacetyl aspartate), MMPR (6-methylmercaptopurine riboside), 6AN (6-aminonicotinamide); referred to as PMA] is an effective radiation (XRT) sensitizer. Using the MCF-7 human mammary tumor, we detected 6-phosphogluconate (6PG), an intermediate in the pentose phosphate pathway, and a reduction in nucleoside triphosphates after treatment with PMA in vivo. In vivo studies indicated that PMA induces a tumor response as evidenced by an increase in tumor growth delay from 10.2 +/- 4.6 (control) to 29.3 +/- 6.7 days. Neither PMA nor XRT alone induced tumor shrinkage. PMA→ 5 Gy induced tumor shrinkage and after 33 days the tumors had not attained their pretreatment volume. By day 51, the mice still had not doubled their tumor volume, indicating that PMA is an active regimen in human tumors, and an effective XRT sensitizer. We also investigated the efficacy of combining with paclitaxel with bryostatin. Bryostatin 1, if administered first, decreased the efficacy of paclitaxel but if administered after paclitaxel moderately enhanced ($p<0.05$) tumor growth delay compared to paclitaxel alone. Further studies suggested that this could be due to changes in pH, blood flow, or cells traversing mitosis.

14. SUBJECT TERMS
Breast Cancer, Imaging, Axilla, Lymph Nodes, MRI, Clinical Trials, Humans
Radiation, biochemical modulation, NMR spectroscopy

15. NUMBER OF PAGES
34

16. PRICE CODE

17. SECURITY CLASSIFICATION OF REPORT	18. SECURITY CLASSIFICATION OF THIS PAGE	19. SECURITY CLASSIFICATION OF ABSTRACT	20. LIMITATION OF ABSTRACT
Unclassified	Unclassified	Unclassified	Unlimited

NSN 7540-01-280-5500

Standard Form 298 (Rev. 2-89)
Prescribed by ANSI Std. Z39-18
298-102

FOREWORD

Opinions, interpretations, conclusions and recommendations are those of the author and are not necessarily endorsed by the U.S. Army.

_____ Where copyrighted material is quoted, permission has been obtained to use such material.

_____ Where material from documents designated for limited distribution is quoted, permission has been obtained to use the material.

_____ Citations of commercial organizations and trade names in this report do not constitute an official Department of Army endorsement or approval of the products or services of these organizations.

__✓__ In conducting research using animals, the investigator(s) adhered to the "Guide for the Care and Use of Laboratory Animals," prepared by the Committee on Care and use of Laboratory Animals of the Institute of Laboratory Resources, national Research Council (NIH Publication No. 86-23, Revised 1985).

__✓__ For the protection of human subjects, the investigator(s) adhered to policies of applicable Federal Law 45 CFR 46.

__✓__ In conducting research utilizing recombinant DNA technology, the investigator(s) adhered to current guidelines promulgated by the National Institutes of Health.

__✓__ In the conduct of research utilizing recombinant DNA, the investigator(s) adhered to the NIH Guidelines for Research Involving Recombinant DNA Molecules.

_____ In the conduct of research involving hazardous organisms, the investigator(s) adhered to the CDC-NIH Guide for Biosafety in Microbiological and Biomedical Laboratories.

_____   10/13/99
PI - Signature   Date

Table of Contents

Introduction

Recent Studies (past 2 years)

Previous studies by this investigator have shown that PMA[PALA + MMPR + 6AN [PALA (n-phosphonacetyl aspartate), MMPR (6-methylmercaptopurine riboside), 6AN (6-aminonicotinamide); referred to as PMA] is an effective radiosensitizer and enhances chemotherapy in two tumor models (1-5). In addition, we have shown that 6AN enhances the effect of radiation on RIF-1 fibrosarcoma cells (6,7). This enhancement has been shown to be sequence dependent, i.e. if the radiation is administered prior to 6AN there is no enhancement. A criticism of the study that has been done was that the study was done in murine tumors; the NIH has suggested that human tumors need to be studied. Thus the goal of the current studies are to

1. Determine if 6AN enhances the effects of radiation in cell culture with a human tumor model.
2. Reproduce our previous murine tumor data (NMR (nuclear magnetic resonance) and tumor growth delay studies) in a human tumor (in vivo) using PMA.

In addition, In addition, we investigated the efficacy of combining paclitaxel with bryostatin to increase its efficacy. Paclitaxel is a very effective agent for treating human breast cancers. This study was designed to enhance its efficacy by the addition of bryostatin 1.

Previous Studies

1. Initial studies were focused on determining the utility of contrast enhanced magnetic resonance imaging of lymph nodes to detect tumor and discriminate between inflammatory and malignant nodes. This was the initial goal proposed in the initial application. R3230AC mammary carcinoma and inflammation (Freund's adjuvant) were induced on the superior aspect of the foot as initially proposed (the Army had initially insisted on a different location). It was decided to try several newer pulse sequences so a total of 8 sequences instead of the original 2 were obtained on all rats studied. The Contrast to Noise Ratio (CNR) relative to muscle was measured pre and post injection of Combidex to determine if the injection of this agent enhanced the discrimination between tumor and adjacent tissue, compared to and inflammatory lesion.

Body

<u>Recent studies – Enhancement of Tumor Response to Radiation and Chemotherapy</u>

In the previous report it was noted that studies were begun with the MCF-7 tumor model, both in vivo and in vitro. These studies are described below.

In vitro studies have been done with 6AN using the MCF-7 human mammary carcinoma. These studies utilized previously published techniques used by these investigators (6,7). It was demonstrated that the cells were stable in the NMR perfusion system for extended periods of time. In contrast, spectra obtained on MCF-7 cells treated with 6AN showed a decrease in phosphocreatine (PCr) and nucleoside triphosphates (NTP) (Fig. 1). The results are similar to previous studies of the RIF-1 results except that there is a decrease in NTP. Previous studies with RIF-1 used both a 15 hour exposure (6) and a 4 hour exposure (7). The 4 hour study was deemed more appropriate since shorter infusions would be more relevant clinically. Surviving fraction studies were done on the MCF-7 cells using a 4 hour exposure using previously described techniques (6,7). 6AN by itself, over the dose range of 40-240 uM showed no effect on survival as expected (Fig. 2). This is similar to our results with RIF-1 cells wherein 6AN alone had no effect on surviving fraction. Longer incubations did show that 6AN was toxic; twenty four hours of exposure to 6AN resulted in enhanced cell kill compared to controls. Cell survival studies showed that there was enhanced cell kill (compared to radiation alone or XRT→6AN) if 6AN was administered before radiation. The surviving fraction after 4 Gy was 0.087 +/- 0.007 compared to 0.036 +/- 0.018 for cells exposed to 6AN before radiation (Appendix 2). Further studies done in this interval demonstrated an enhanced effect of adriamycin in cells pretreated with 6AN, but not with paclitaxel. These studies are being pursued further with flow cytometry to determine if metabolic inhibition by 6AN could have induced a change in the cell cycle distribution (appendix 2). The activity of paclitaxel is dependent on cells entering mitosis.

The major emphasis during the past year has been in perfecting and performing the in vivo studies. Our initial studies utilized a dose of 6AN of 10mg/kg, which had not been toxic in CD8F1 mice. However, as noted in the previous report, this was toxic in nude mice. An extensive series of studies were done to determine the maximum tolerated dose of 6AN when keeping PALA and 6-methylmercpatpurine riboside (MMPR) fixed. (PALA - 100mg/kg, MMPR - 150mg/kg). Tumors were transplanted in the mammary fat pad (orthotopic site) as recommended by the site visit team. The tumors typically required approximately 6 weeks to grow to a volume of approximately 200 mm3, the minimum size that is feasible for 31P NMR studies. The mice were also implanted with a time release estrogen pellet since the MCF-7 is estrogen dependent. Chemotherapy and radiation were administered as previously published (1-4). The NMR studies were presented in last year's report and are included (Fig. 3). As was noted for the two murine tumors studied previously, PALA + MMPR + 6AN (PMA) caused an increase in 6-phosphogluconate (6PG) (otherwise undetectable) and a decrease in high energy phosphates.

Initial studies with PALA, MMPR, 6AN with 6AN administered at 10mg/kg demonstrated a mortality of approximately 30% on multiple studies. Previous studies (D.S. Martin

unpublished) had suggested that the most toxic of the drugs was 6AN and therefore a dose titration study was done. Studies with 6AN at 8mg/kg were similarly beyond the maximum tolerated dose (mortality >10%). The highest feasible dose was shown to be 6mg/kg when administered in combination with PALA and MMPR.

Subsequent to determining the maximum tolerated dose of 6AN for the three drug combination, we studied the effect of the three drugs in enhancing radiation. Figure 4 summarizes a recent study demonstrating this effect. Tumor bearing mice (~ 200mm3) were treated with saline (control), 5 Gy alone (single fraction), PALA, MMPR, 6AN (single dose), PMA→ 5 Gy, or PMA→ 10 Gy and tumor burden monitored subsequently. Figure 2 shows the effects of treatment on tumor volume. Control mice had a doubling time of 10.2 +/- 4.6 days. A single fraction of 5 Gy has little effect on tumor growth as expected, resulting in a tumor doubling time of 17.0 +/- 5.1 days. A single course of PMA does not result in tumor shrinkage although there is a clear decrease in tumor growth rate with a doubling time of 29.3 +/-6.7 days. Treatment with PMA + 5 Gy or 10 Gy results in tumor shrinkage. In contrast to 5 Gy alone which does not result in tumor shrinkage, treatment with PMA + 5Gy results in tumor shrinkage and the time for the tumor to attain its pretreatment volume is ~ 35 days. If one compares tumor volumes at 28 days the difference in tumor volumes are highly significant (p<0.01). At day 35, two of the mice had not regrown to their pretreatment tumor volume. The mice were followed to day 51 without mortality and without the tumor having attained double its initial volume. Two mice died subsequently and the experiment was terminated. Previously we have "autopsied" several mice bearing MCF-7 and estrogen pellets who died with minimal tumor burden. They frequently had enlarged uteruses which impinged on the bladder and may have led to uro-sepsis as a possible explanation of these unexpected deaths. However, the data are clear that PMA→radiation is superior therapy compared to radiation alone.

In addition, the effect of Bryostatin 1, a Protein Kinase C inhibitor, on tumor metabolism, growth, blood flow, cell cycle events, and tumor response to a combination of Bryostatin 1 and paclitaxel was investigated in a murine mammary carcinoma. The maximum tolerated dose of Bryostatin 1 i.p. was found to be 80ug/kg. This resulted in a small but significant (p<0.05) increase in tumor doubling time (4.2 $\pm$ 0.3 days) compared to control tumors (3.0 $\pm$ 0.3 days). A dose of 100ug/kg resulted in a greater tumor doubling time (6.9 $\pm$ 0.1days) but with unacceptable mortality. 31P NMR spectra showed a decrease in pH and high energy phosphates (as measured by the ratio of PCr:Pi) at 12 and 24 hours after treatment with Bryostatin 1(80ug/kg) (see Appendix 1). Mice treated with paclitaxel, administered at a dose of 12mg/kg q12h x 3 weekly for 3 weeks had a tumor doubling time of 23.4 $\pm$ 1.7 days. Mice pretreated with Bryostatin 1 (80ug/kg) followed 12 hours later by paclitaxel (12mg/kg q12h x 3) weekly x 3 weeks had a tumor doubling time of 9.7$\pm$1.1 days. This was significantly less (p < .001) than paclitaxel alone indicating an inhibitory effect by Bryostatin 1 on paclitaxel therapy. In comparison, tumor bearing mice treated with the same dose but with the sequence of paclitaxel→Bryostatin 1, had a tumor doubling time of 29.6 $\pm$ 0.6 days. This was significantly greater (p<0.05) than the tumor doubling times for the other two cohorts, demonstrating the sequence dependence of this combination. Perfusion studies using dynamic enhanced magnetic resonance imaging demonstrated significantly decreased tumor uptake of Gd-DTPA after treatment with Bryostatin 1 at a dose of 80 ug/kg (p<0.05). The efficacy of paclitaxel is dependent on metaphase arrest which requires activation of p34^{cdc2} kinase activity. Treatment with paclitaxel increased p34^{cdc2}

kinase activity, whereas administration of Bryostatin 1 before paclitaxel prevented the p34^{cdc2} kinase activitation by paclitaxel. In vitro, paclitaxel induced mitotic block in MKN-74 human gastric cancer cells as determined by MPM-2 labeling. Pretreatment with Bryostatin 1 prevented cells from entering mitosis and a significantly lower mitotic index was observed after treatment with paclitaxel. These data indicate that sequence is critical in combining paclitaxel and Bryostatin 1 and suggest that the inhibition of tumor response to paclitaxel by Bryostatin 1 is multifactorial including such diverse factors as decreased blood flow and inhibition of entry into mitosis by paclitaxel (see Appendices 1,4). These data were sued for developing the drug sequence for clinical trials with bryostatin 1 and paclitaxel which are now ongoing.

Diagnostic Studies of Contrast Enhanced Magnetic Resonance Lymphography (Reported in previous reports)

R3230AC mammary carcinoma and Freund's adjuvant were injected on the superior aspect of the foot as initially proposed. It was decided to try several additional pulse sequences so a total of 8 sequences instead of the original 2 were obtained on all rats studied. The Contrast to Noise Ratio (CNR) relative to muscle was measured pre and post injection of Combidex to determine if the injection of this agent enhanced the discrimination between tumor and adjacent tissue, compared to and inflammatory lesion. Table 1 is a list of pulse sequences studied and Table 2 summarizes the percent tumor for the tumor bearing rats studied, based on histopathologic analyses. Corresponding data is not presented for the inflammatory nodes since they were virtually 100% inflammatory. Tumor nodes were between 4 and 6 mm at the time of study. Imaging parameters included field of view = 80 x 80 mm, 128 x 256 in plane resolution, 2 mm thick slices with a 0.5 mm gap between slices.

Statistically significant changes in CNR were observed for the FSE sequences at all three echo train lengths. None of the other pulse sequences produced significant changes in CNR between tumor and inflammatory nodes. Despite the statistically significant changes in CNR seen with the fast spin echo (FSE) sequences, there is significant overlap between tumor and inflammatory nodes.

The likely explanation for the unsuccessful outcome lies in the size of the tumor. In a previous study from this laboratory using a prostate tumor model, excellent differentiation was noted between tumor and inflammatory nodes. Those nodes were typically 13-14 mm. In contrast, these experiments utilized a different tumor, but also the size of the nodes were between 4 and 6 mm. These small nodes, with a wide diversity of tumor involvement, often showed evidence of inflammation as part of the metastatic process. It is likely that the presence of both inflammation and tumor has led to the poor results of the study (Appendix 3).

Legends

Fig. 1. In vitro 31P NMR spectra of MCF-7 cells perfused with 6AN for 4 hours. Note the appearance of 6PG and the decrease in phosphocreatine. A. Before 6AN. B. Post 6AN infusion. Each spectrum required 4.5 hours. Time points are from 6AN infusion. A=6-phosphogluconate, B= phosphoethanolamine, C=phosphocholine, D=inorganic phosphate, E=glycerophosphoethanolamine, F=glycerophosphocholine, G=phosphocreatine, H=γ nucleoside triphosphate (NTP), I= α NTP, K=βNTP.

Fig. 2. Surviving fraction studies done on MCF-7 cells at various doses of 6AN for various exposure durations. Note the lack of toxicity of 6AN at 200 uM when exposure is 4 hours.

Fig. 3. In vivo 31P NMR studies of MCF-7 tumors treated with PMA. Peak identifications include A=6-phosphogluconate, B= phosphoethanolamine, C=phosphocholine, D=inorganic phosphate, E=glycerophosphoethanolamine, F=glycerophosphocholine, G=phosphocreatine, H=γ nucleoside triphosphate (NTP), I= α NTP, K=βNTP. Note the appearance of 6PG at 10 and 24 hours and the increase in Pi relative to β NTP.

Fig. 4. Effect of treatment on tumor volume. Note that after treatment with PMA alone or XRT alone, there is no decrease in tumor volume. In contrast, treatment with PMA $\rightarrow$XRT (5 or 10 Gy) results in tumor shrinkage and a significantly greater effect.
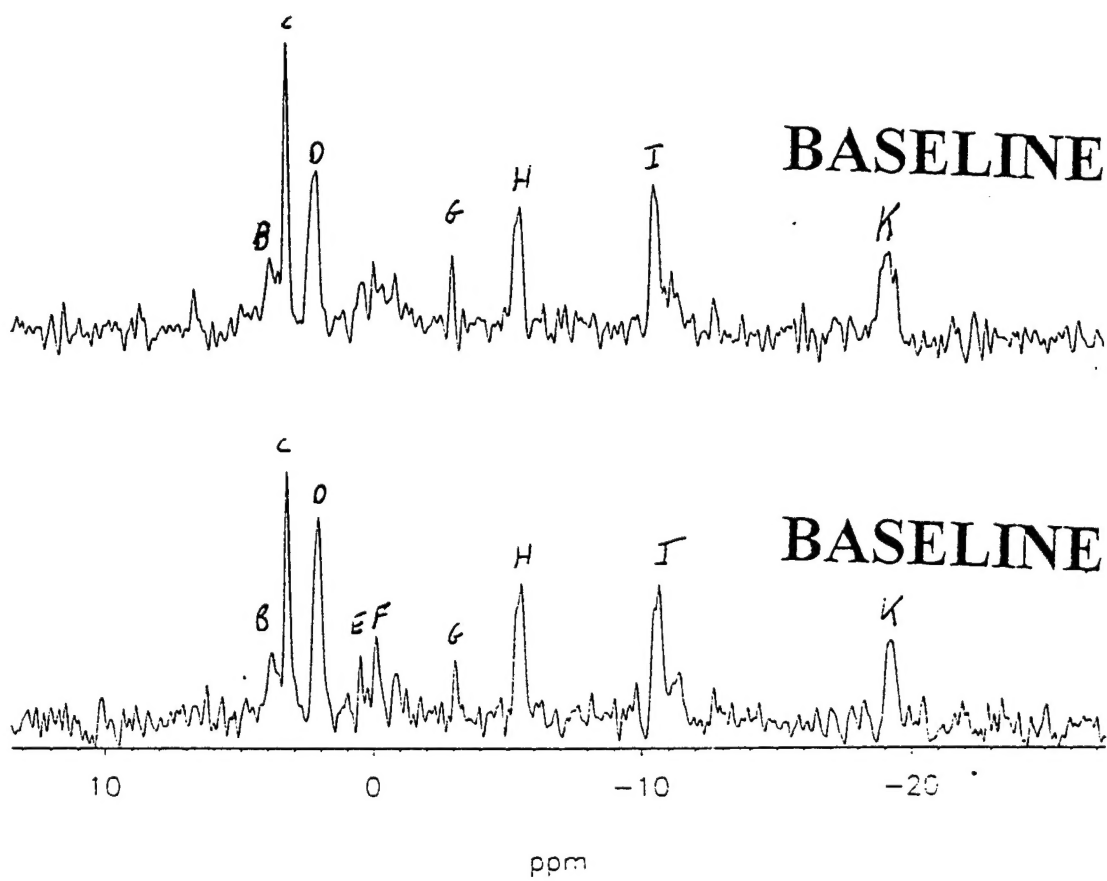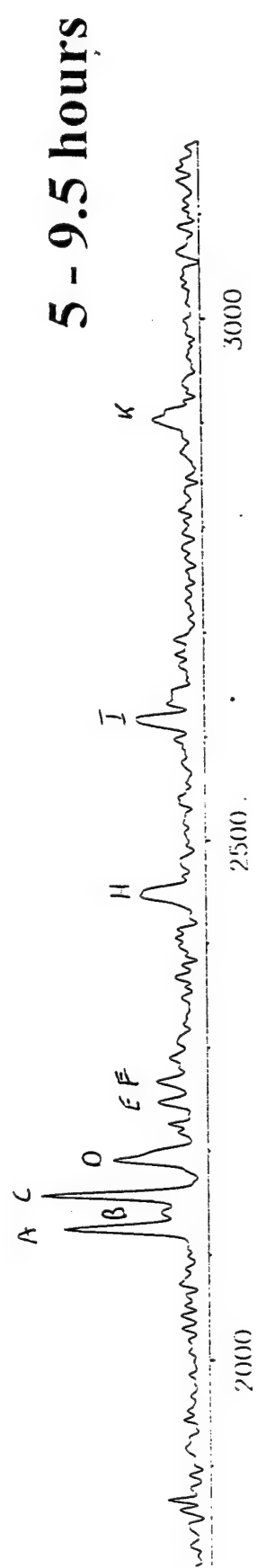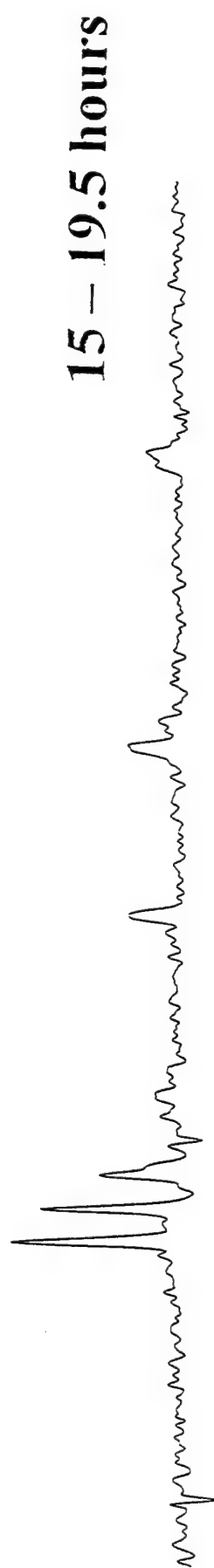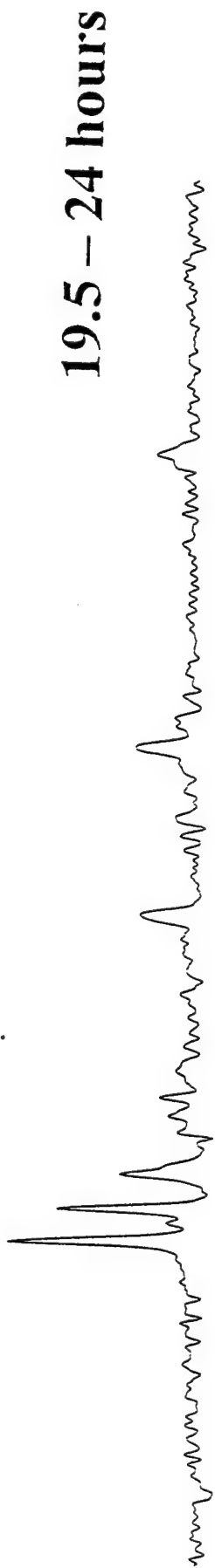
Figure 1A

19.5 – 24 hours

15 – 19.5 hours

9.5 – 14 hours

5 – 9.5 hours

3000
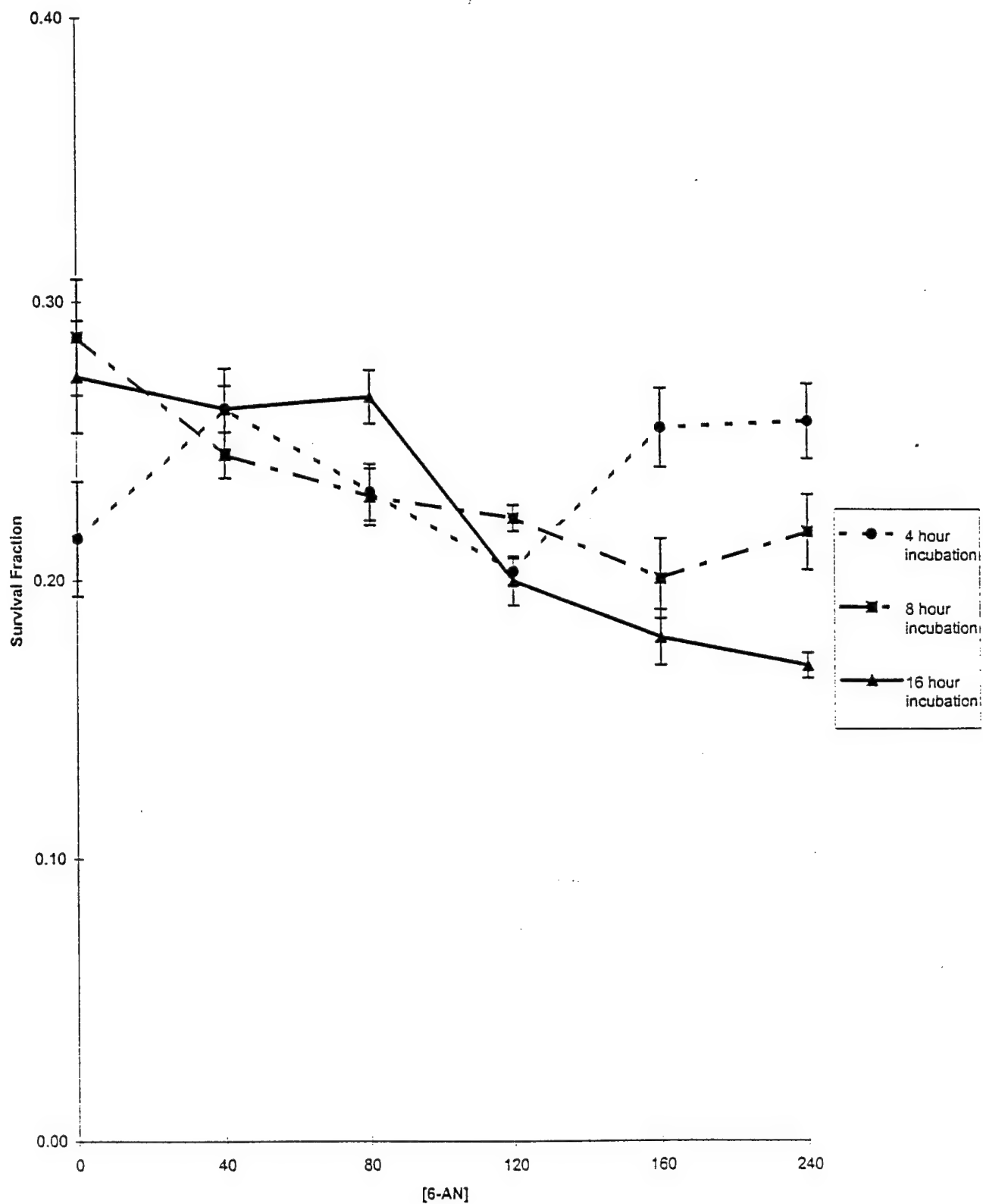
2500

2000

points

Figure 1B

Effect of 6-AN on MCF-7 cell survival

Figure 2
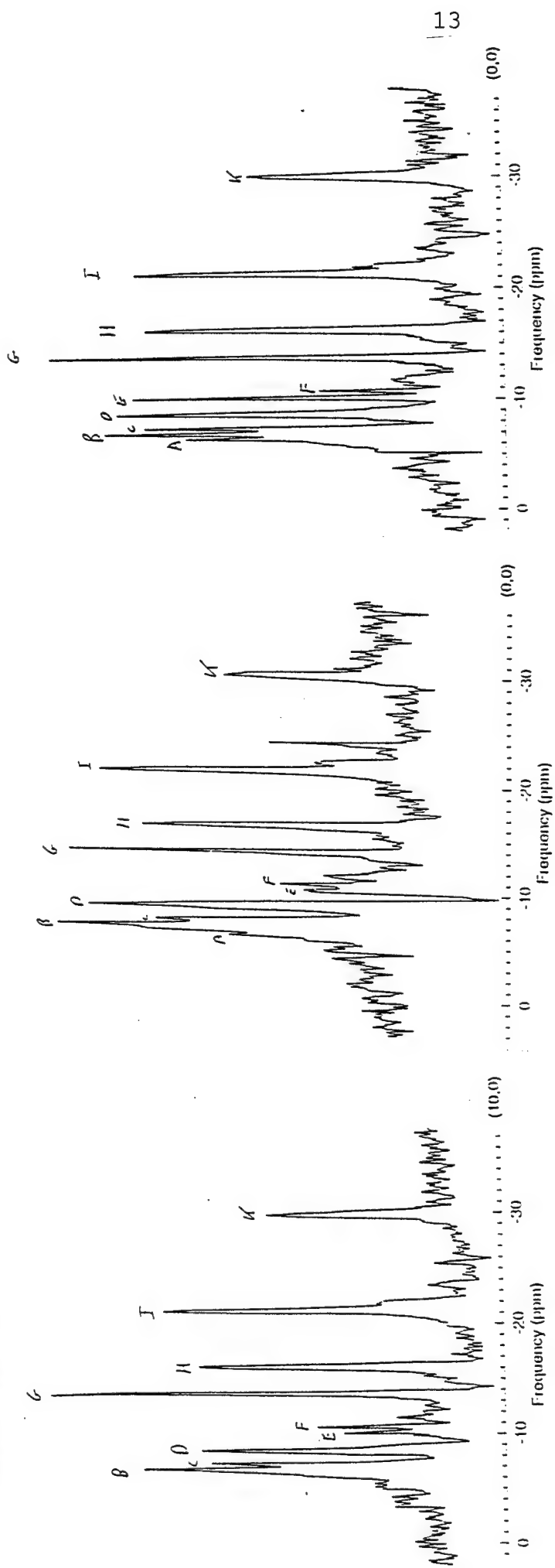
Figure 3

Figure 4

The effects of radiation and PMA on MCF-7 Breast Cancer Xenografts Tumor
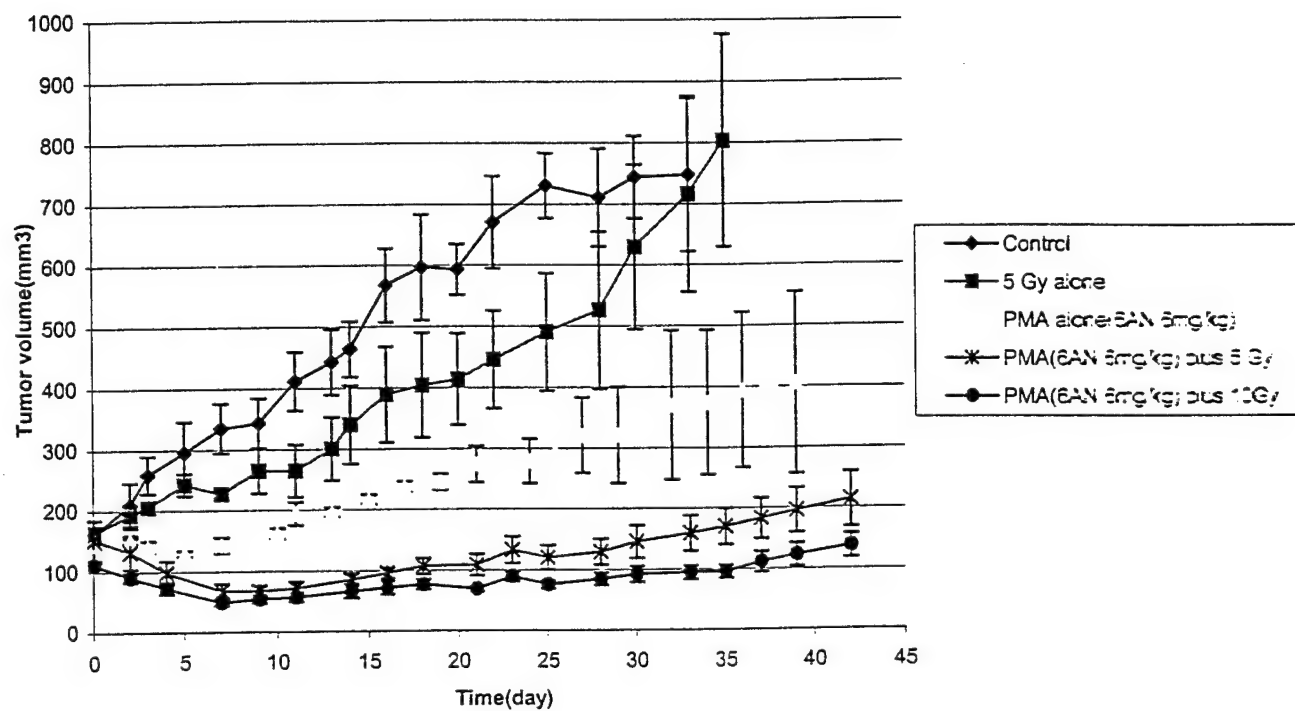
Table 1

Pulse Sequences	TR/TE
T2 weighted Fast Spin Echo(FSE)	4000/105
Echo train length (ETL) = 8,16,32	
Proton Density (PD) Fast Spin Echo	4000/15
Echo Train Length = 8, 16,32	
Gradient Recalled Echo (GRE)	150/20
T2 weighted conventional spin echo (CSE)	2000/20,80

Table 2

Animal #	Per Cent Tumor/Pathologic Evaluation
1	0
2	95
3	5 (very reactive)
4	0 (all reactive)
5	Tumor outside node; no tumor in the node
6	95
7	95 – necrotic
8	100
9	100
10	85
21	100
22	95
23	5
24	95 – necrotic
25	55 –inside tumor; tumor also outside node
26	85
27	100
28	100
31	40
32	95
33	95
34	75

Key Research Accomplishments

1. Demonstration in vitro that 6AN enhances radiation and adriamycin efficacy but not paclitaxel.
2. Determination of a safe dose of 6AN in combination with PALA and MMPR for immunodeficient mice bearing human tumors.
3. Demonstration that PALA, MMPR, 6AN enhances the efficacy of radiation in human tumors and also has anti-neoplastic efficacy in the absence of radiation.
4. Demonstrated that the efficacy of the combination of Paclitaxel and bryostatin-1 is sequence dependent. Treatment with bryostatin 1 prior to paclitaxel can inhibit the efficacy of paclitaxel. <u>This has been the rationale for drug sequencing in current clijcnial trials with bryostatin 1 and paclitaxel</u>.
5. Several possible etiologies including decreased blood flow, pH, energy metabolism and mitotic entry are presented for the antagonism of Paclitaxel by bryostatin 1

Reportable Outcomes

Abstracts
1. Holleran A, Chen Y, and Koutcher JA. Effect of 6-Aminonicotinamide on human tumor metabolism and response to radiation and chemotherapy. 7th Mtg of Int Society for Magn. Resonance in Med. Phil, Pa. May 1999
2. Koutcher JA, Matei C, Zakian K, Ballon D, and Schwartz GK. In vivo metabolic and tumor growth delay studies with paclitaxel and bryostatin 1, a PKC inhibitor. Amer Assoc Cancer Research. 89th Ann Mtg, New Orleans 1998. Abstract 1304
3. Schwartz LH, Koutcher JA, Matei C, Fischer, R, and McLachlin SJ. MR imagin with superparmagnetic iron oxide. Radiological Society of N. America, Chicago Illinois, 1997 Abstract #1273

Papers
1. Koutcher JA, Motwani M, Zakian KL, Li X-K, Matei J, Ballon D, Yoo HH and Schwartz GK. The in vivo effect of bryostatin 1 on paclitaxel induced tumor growth, mitotoic entry and blood flow. Clinical Cancer Res. Submitted

Funding Applied for Based on This Work

Conclusions

The research that was funded in this proposal consisted of three projects. Due to changes in the animal model insisted upon by the Army, the initial study of an iron oxide contrast agent could not be done since tumors grew very poorly. This has been summarized in a previous report. AMI-227 results in an increase in contrast between tumor bearing and inflammatory nodes, particularly using the fast spin echo sequence. However, in this study, wherein small nodes were studied (in contrast to a previous study wherein nodes ~14 mm were studied), there is significant overlap in the contrast-to-noise ratio between tumor and inflammatory nodes. This is likely to be due to the study of smaller nodes, since there is an inflammatory component to the tumor bearing nodes. In the small nodes, this inflammatory component may result in lack of discrimination between tumor bearing and inflammatory nodes. but in essence the limited data obtained did not suggest that this agent could be used to detect metastatic breast cancer in lymph nodes as a staging technique.

The second research project that was funded by this award was to determine if the combination of PALA, MMPR 6AN enhances the effect of radiation. The latter drug combination required a decrease in 6AN to decrease toxicity. With a dose of 6AN of 6mg/kg, it was shown in the human mammary carcinoma, that the three drug combination enhanced the efficacy of radiation, in addition to inducing a tumor growth delay without radiation.

In addition, we investigated the efficacy of combining with paclitaxel with bryostatin to increase its efficacy. Bryostatin 1, if administered first, decreased the efficacy of paclitaxel. Tumor doubling time was moderately enhanced ($p<0.05$) compared to pactlitaxel alone if bryostatin 1 was administered after paclitaxel. Further studies suggested that this could be due to changes in pH, blood flow, or cells traversing mitosis.

References

1. Koutcher JA, Alfieri AA, Stolfi RL, Devitt ML, Colofiore JR and Martin DS. Potentiation of a three drug chemotherapy regimen by radiation. Cancer Research 53: 3518-3523, 1993.

2. Koutcher JA, Alfieri AA, Tsai JC, Matei C, Stolfi, RL, Ballon D, and Martin DS. Evaluation of chemotherapy and radiation enhancement and 31P NMR spectral changes induced by biochemical modulation. Cancer Investigation. 15: 111-120, 1997.

3. Koutcher JA, Alfieri, AA, Thaler H, Matei, C, and Martin DS. Radiation Enhancement by Biochemical Modulation and 5-Fluorouracil. Int. J. Rad. Onc. Biol. and Physics. 39:1145-1152, 1997.

4. Nord LD, Stolfi RL, Alfieri AA, Netto G, Reuter V, Sternberg SS, Colofiore JR, Koutcher JA, and Martin DS. Apoptosis induced in advanced CD8F1-murine mammary tumors by the combination of PALA, MMPR and 6AN precedes tumor regression and is preceded by ATP depletion. Cancer Chemotherapy and Pharmacology. 40:376-384, 1997.

5. Mahmood U, Street JC, Matei CM, Ballon D, Martin DS, and Koutcher JA. In vivo detection of pentose phosphate pathway blockade secondary to biochemical modulation. NMR in Biomedicine. 9: 114-120, 1996

6. Street JC, Mahmood U, Ballon D, Alfieri A, and Koutcher JA. 13C and 31P NMR investigation of effect of 6-Aminonicotinamide on metabolism of RIF-1 tumour cells in vitro. J. of Biol. Chem. 271:4113-4119, 1996.

7. Street JC, Alfieri AA, and Koutcher JA. Quantitation of metabolic and radiobiological effects of 6-Aminonicotinamide in RIF-1 tumor cells in vitro. Cancer Res. 57: 3956-3962, 1997.

8. Koutcher JA, Alfieri AA, Matei, CM, Meyer KL, Street JC, and Martin DS. In vivo 31P NMR detection of Pentose Phosphate Pathway block and enhancement of radiation sensitivity with 6-aminonicotinamide. Magnetic Resonance Med. 36: 887-892, 1996

Final Report

A. Bibliography

Abstracts

4. Holleran A, Chen Y, and Koutcher JA. Effect of 6-Aminonicotinamide on human tumor metabolism and response to radiation and chemotherapy. 7th Mtg of Int Society for Magn. Resonance in Med. Phil, Pa. May 1999
5. Koutcher JA, Matei C, Zakian K, Ballon D, and Schwartz GK. In vivo metabolic and tumor growth delay studies with paclitaxel and bryostatin 1, a PKC inhibitor. Amer Assoc Cancer Research. 89th Ann Mtg, New Orleans 1998. Abstract 1304
6. Schwartz LH, Koutcher JA, Matei C, Fischer, R, and McLachlin SJ. MR imaging with superparmagnetic iron oxide. Radiological Society of N. America, Chicago Illinois, 1997 Abstract #1273

Papers
1. Koutcher JA, Motwani M, Zakian KL, Li X-K, Matei J, Ballon D, Yoo HH and Schwartz GK. The in vivo effect of bryostatin 1 on paclitaxel induced tumor growth, mitotoic entry and blood flow. Clinical Cancer Res. Submitted

B. List of personnel who received funding from this project

1. Jason A. Koutcher
2. James Street
3. Anne Holleran

The *in Vivo* Effect of Bryostatin-1 on Paclitaxel-induced Tumor Growth, Mitotic Entry, and Blood Flow[1]

Jason A. Koutcher, Monica Motwani, Kristen L. Zakian, Xiao-Kui Li, Cornelia Matei, Jonathan P. Dyke, Douglas Ballon, Hyok He Yoo, and Gary K. Schwartz[2]

Departments of Medical Physics [J. A. K., K. L. Z., J. P. D., D. B.], Radiology [J. A. K., C. M., D. B., H. H. Y.], and Medicine [J. A. K., G. K. S.], and Laboratory of Gastrointestinal Oncology and New Drug Development [M. M., X-K. L., G. K. S.], Memorial Sloan-Kettering Cancer Center, New York, New York 10021

ABSTRACT

Pretreatment of tumor cells with the protein kinase C (PKC) inhibitor bryostatin-1 enhances the cytotoxicity of most chemotherapeutic agents. However, in the case of paclitaxel, this effect has been shown *in vitro* to be best achieved when bryostatin-1 follows (rather than precedes) paclitaxel treatment. With combination trials of bryostatin-1 and paclitaxel planned for clinical trials and with only *in vitro* data available regarding drug sequence, we elected to undertake an *in vivo* study evaluating the effect of sequential bryostatin-1 and paclitaxel in a tumor-bearing mouse model and to correlate this effect to cell cycle events, tumor metabolism, and tumor blood flow. At the maximum tolerated i.p. dose, bryostatin-1 at 80 μg/kg resulted in a small but significant increase in tumor doubling time (4.2 ± 0.3 days) compared with control tumors (3.0 ± 0.3 days; $P < 0.01$). Mice treated with i.v. paclitaxel, administered at a dose of 12 mg/kg every 12 h for three doses, weekly for 3 weeks, had a tumor doubling time of 23.4 ± 1.7 days. Mice pretreated with i.p. bryostatin-1 (80 μg/kg) followed 12 h later by i.v. paclitaxel (12 mg/kg every 12h for three doses) weekly for 3 weeks had a tumor doubling time of 9.7 ± 1.1 days. This was significantly less ($P < .001$) than paclitaxel alone, which indicated an inhibitory effect by bryostatin-1 on paclitaxel therapy. In comparison, tumor-bearing mice that were treated with the same dose but with the sequence of paclitaxel followed by bryostatin-1 had a tumor doubling time of 29.6 ± 0.6 days. This was significantly greater than the tumor doubling times for any condition tested ($P < 0.01$), demonstrating the sequence dependence of this combination. The efficacy of paclitaxel is dependent on mitotic entry, a step that requires activation of $p34^{cdc2}$ kinase activity. Treatment with paclitaxel *in vivo* increased $p34^{cdc2}$ kinase activity in the mouse mammary tumors, whereas administration of bryostatin-1 before paclitaxel prevented the $p34^{cdc2}$ kinase activation by paclitaxel. This was further evaluated *in vitro* by flow cytometry in MKN-74 human gastric cancer cells. As determined by MPM-2 labeling, which identifies cells in mitosis, pretreatment with bryostatin-1 prevented paclitaxel-treated cells from entering mitosis. Bryostatin-1 has been reported to induce changes in muscle metabolism and to decrease muscle blood flow. These events could impact on the interaction of bryostatin-1 with paclitaxel. Using proton-decoupled phosphorus nuclear magnetic resonance (^{31}P-NMR) spectroscopy *in vivo*, bryostatin-1 at 80 μg/kg induced a decrease in both intratumoral pH and high-energy phosphates. *In vivo* perfusion studies, using dynamic enhanced NMR imaging with gadolinium diethylenetriamine pentaacetic acid, also demonstrated decreased tumor blood flow. These studies suggest that the inhibition of tumor response to paclitaxel by bryostatin-1 is multifactorial and includes such diverse factors as inhibition of cell entry into mitosis, a decrease in pH and energy metabolism, and a decrease in tumor blood flow. These results indicate that, as this combination enters Phase I clinical trials, the sequence of paclitaxel followed by bryostatin-1 will be critical in the clinical trial design.

INTRODUCTION

Bryostatin-1 is a macrocyclic lactone obtained from the marine bryozoan, Buglia Neritina. *In vitro* single-agent activity has been demonstrated against B16 melanoma, M5076 reticulum sarcoma, and L10A B-cell lymphoma (1, 2). Activity *in vitro* has also been observed in human A549 lung and MCF-7 breast cancer cells (3). Although the exact mechanism of action of bryostatin-1 is unknown, it has been shown *in vitro* to activate PKC[3] activity with short-term exposure, by inducing translocation of the protein from its cytoplasmic to its membrane-associated active fraction. Conversely, prolonged exposure results in membrane depletion of PKC and results in inactivation of the PKC activity (4). Previous studies (5–10) have suggested that PKC inhibitors may have antineoplastic activity by mechanisms

[3] The abbreviations used are: PKC, protein kinase C; MR, magnetic resonance; NMR, nuclear MR; CDK, cyclin-dependent kinase; Gd-DTPA, gadolinium diethylenetriamine pentaacetic acid; LD10, dose that kills 10% of mice; Ara-C, 1-β-D-arabinofuranosylcytosine; TDT, tumor doubling time; PCr, phosphocreatine; Pi, inorganic phosphate; ROI, region(s) of interest.

other than PKC inhibition. For example, the inhibition of cell growth by bryostatin-1 has also been correlated with the induction of p21 protein expression and the inhibition of CDK_2 activity (5). In clinical trials, bryostatin-1 has also been associated with the release of tumor necrosis factor, the stimulation of interleukin 2, and an increase in interleukin 6 (7, 8). It has also been shown in muscle to induce changes in energy metabolism, decrease proton efflux, and reduce muscle blood flow (9, 10).

Bryostatin-1 has completed Phase I clinical trials, and different schedules of administration have been tested (11–13). Doses of bryostatin-1 above 65 μg/m^2 were associated with significant myalgias (12), the etiology of which remain unclear, although blood-flow inhibition was postulated as a likely candidate (9, 10). A bryostatin-1 dose of 25–50 μg/m^2 seems to be well tolerated and can be administered on a schedule of 3 out of every 4 weeks without dose-limiting toxicity. However, despite extensive Phase 1 testing, the results with single-agent bryostatin-1 have been discouraging. Limited responses have been observed in patients with ovarian carcinoma and lymphoma (11). The ultimate success of this agent may depend on new directions in its development.

Several reports indicate that inhibitors of PKC can significantly enhance the activity of chemotherapeutic agents. Bryostatin-1 has been shown to enhance the induction of apoptosis by Ara-C in HL-60 cells (14). The effect was best achieved when the cells were first treated with bryostatin-1 and then, 24 h later, treated with Ara-C. The enhancement of apoptosis, as determined by DNA fragmentation under these conditions, correlated with the enhanced inhibition of tumor growth as determined by clonogenic assays. Similar results have been reported with bryostatin-1 on the vincristine-treated WSU-DLC2 diffuse large-cell lymphoma cell line cells (15, 16) and on cisplatin-treated ovarian cancer cells (17). As in the case with Ara-C, this result was best achieved when bryostatin-1 treatment preceded that of either vincristine or cisplatin.

The sequential nature of this therapeutic approach in enhancing the effectiveness of a chemotherapeutic agent would clearly suggest that bryostatin-1 therapy should precede the cytotoxic agent under investigation. However this may not be the case for all drugs. Bryostatin-1 treatment *in vitro* has been reported to enhance the cytotoxicity of paclitaxel in human U937 leukemic cells only when bryostatin-1 followed paclitaxel treatment (18). This may be related to specific interactions between bryostatin-1 and paclitaxel-treated cells that are independent of bryostatin's effect on PKC. *In vitro* studies with another PKC inhibitor, flavopiridol, have indicated that pretreatment of gastric and breast cancer cells with flavopiridol before paclitaxel will antagonize, rather than synergize, the paclitaxel effect. This antagonism by flavopiridol seems related to the inhibition by flavopiridol on paclitaxel-induced p34^{cdc2} kinase activity (19). The activation of cyclin B$_1$-associated p34^{cdc2} kinase is critical for the effect of single- agent paclitaxel. Because bryostatin-1 is also a CDK inhibitor, we hypothesized that the antagonism of bryostatin-1 on paclitaxel-treated cells may also be related to bryostatin-1's inhibition of paclitaxel-induced p34^{cdc2} kinase activity.

With combination trials of bryostatin-1 and paclitaxel planned for clinical trials and with only *in vitro* data available regarding drug sequence, we elected to undertake a study eval-uating the effect of sequential bryostatin-1 and paclitaxel in a tumor-bearing mouse model. Toward this end, we have treated mice bearing a mouse mammary carcinoma with bryostatin-1 and paclitaxel alone or in sequential combinations (*i.e.,* bryostatin-1 followed by paclitaxel or paclitaxel followed by bryostatin-1) and followed them for tumor growth. We selected a schedule of 3 out of 4 weeks because this has been shown to be safe and well tolerated in the clinical setting. We have also analyzed these tumors for p34^{cdc2} kinase activation, as well as for cyclin B$_1$ protein expression, to determine the effects of these drugs on cell cycle events associated with mitotic arrest induced by paclitaxel. In view of the reported effects of bryostatin-1 on muscle metabolism with associated changes in ATP and a decrease in blood flow, we also elected to use MR spectroscopy (NMR) to serially measure *in vivo* the effects of bryostatin-1 on intratumoral energy, pH, and blood flow.

MATERIALS AND METHODS

In Vivo **Tumor Model.** MCa tumors were removed aseptically from tumor-bearing animals by previously described techniques (20). Briefly, a single-cell suspension was prepared by teasing and abrasion against stainless steel mesh immersed in iced MEM (Earle's balanced salt solution) containing 2% heparin. Cell suspensions were further disrupted by aspiration through an 18-gauge needle, and the final suspension was agitated constantly by a magnetic spin bar. A tumor inoculum of 0.025–0.04 ml (approximately 10^5 cells) was injected s.c. into the dorsum of the foot of male C3H/He mice (Jackson Laboratory, Bar Harbor, Me) with a 26-gauge needle. Greater than 75% of the MCa tumors were viable based on trypan blue exclusion. Tumor volume was estimated from the formula $V = \pi d1 \times d2 \times d3$, where V = volume and $d1$, $d2$, and $d3$ were the three orthogonal diameters. Different cohorts of mice were used for NMR and tumor-growth-delay studies. Mice were fed *ad libitum* until just before NMR and radiation studies.

Cell Culture. The human gastric cancer cell line MKN-74 was used for *in vitro* studies because the MCa tumor cannot be grown *in vitro*. The MKN-74 cell was graciously supplied by Dr. E. Tahara (Hiroshima University, Hiroshima, Japan). Cells were maintained in Eagle's MEMs supplemented with 20% heat-inactivated normal calf serum (Intergen), penicillin, and streptomycin at 37°C in 5% carbon dioxide. The cultures were tested as *Mycoplasma*-free.

Tumor Response and Toxicity Studies. Mice with tumors approximately 100 mm^3 in size were used for both TDT and LD10 (dose that kills 10% of mice) studies. The LD10 studies were done with a single administration of bryostatin-1 i.p. at the doses noted (Table 1). Toxicity was evaluated at day 7 because the tumor had grown to ~700 mm^3 and, therefore, the mice were killed. For evaluation of tumor response for the combined paclitaxel and bryostatin-1 studies, mice were treated with bryostatin-1 (supplied by Bristol-Meyers Squibb, Princeton, NJ) i.p. or paclitaxel (Bristol-Meyers Squibb) i.v. Each cycle of paclitaxel was administered at a dose of 12 mg/kg i.v. for three doses, each separated by 12 h. Mice received: (*a*) saline ($n = 10$); (*b*) bryostatin-1 (80 μg/kg; $n = 10$); (*c*) paclitaxel (12 mg/kg every 12 h for three doses; $n = 10$); (*d*) bryostatin-1 (80 μg/kg) followed 12 h later by the first of three doses of pacli-

taxel (each dose of paclitaxel separated by 12 h; $n = 14$); or (e) paclitaxel (12 mg/kg for three doses, each separated by 12 h, followed by bryostatin-1 (80 μg/kg; 12 h after the last dose of paclitaxel; $n = 14$). The 12-h time interval of administering paclitaxel after the last dose of bryostatin-1 was selected because this was the point at which intratumoral energy and high-energy phosphates were the lowest after bryostatin-1 therapy (see "Results" section, "Effect of Bryostatin-1 on Intratumoral Energy and pH"). For TDT studies of the combinations of paclitaxel and bryostatin-1, the mice received three cycles of each treatment, each separated by 1 week.

p34^{cdc2} Kinase Activity Assay. For these assays, tumors were obtained from all of the sets of animals 12 h after completing day 2 of therapy. Tumors were then homogenized and lysed with buffer containing 50 mM HEPES-KOH (pH 7.5), 150 mM NaCl, 1 mM EDTA, 1 mM NaF, 1 mM DTT, 2.5 mM EGTA, 0.1% Tween 20, 10% glycerol, 10 mM β-glycerophosphate, 0.1 mM Na$_3$VO$_4$, 0.2 mM phenylmethylsulfonyl fluoride, 10 μg/ml aprotinin, and 10 μg/ml leupeptin. The cells were further disrupted by passing through a 21-gauge syringe 10 times and lysates were clarified by centrifugation (10 min at 10,000 × g). Soluble protein (200 μg) was incubated with 1 μg of anticyclin B1 antibody (Santa Cruz Biotechnology Inc., Santa Cruz, CA) at 4°C for 2 h. Immune complexes were then precipitated with 40 μl of immobilized protein A (RepliGen, Weedham, MA) overnight at 4°C, washed three times with lysis buffer and twice with kinase assay buffer [50 mM HEPES-KOH (pH 7.5), 10 mM MgCl$_2$ and β-glycerophosphate, 1 mM DTT, 2.5 mM EGTA, 0.1 mM Na$_3$VO$_4$, 1 μM NaF]. The kinase assay was done by combining the washed protein beads with 20 μl of kinase buffer plus 10 μCi of [γ-^{32}P]ATP, 15 μM ATP, and 50 μg/ml Histone H1 (Boehringer Mannheim, Germany). The reaction was allowed to proceed for 30 min at 30°C and was terminated by adding 10 μl of Laemmli sample buffer and boiling for 5 min. Products were resolved by 10% SDS-PAGE. The incorporated radioactivity was determined by Betascope 603 blot analyzer (Betagen Corp., Waltham, MA).

Immunoblot Analysis. Protein lysates, prepared for kinase assays, were used for immunoblotting. Soluble protein (50 μg) was resolved by 10% SDS-PAGE and transferred onto Immobilion-P membranes (Millipore). The equal loading of proteins was confirmed by Amido Black staining. The membranes were probed with mouse monoclonal cyclin B$_1$ (kindly provided by Dr. Tim Hunt, Imperial Cancer Research Fund Clare Hall Laboratories, United Kingdom). The membrane was treated with a secondary sheep antimouse-horseradish peroxidase antibody for 1 h at room temperature. Detection was done by ECL chemiluminescence reagents (DuPont NEN Life Science Products, Boston, MA) according to the manufacturer's protocol. The levels of expressions were quantified using a densitometric scanning system.

MPM-2/Propidium Iodide Bivariate Flow Cytometry. MKN-74 cells (1.4×10^6/100-mm dish) were cultured for 48 h and treated with paclitaxel (100 nM) as a single agent for 18 h (T$_{18}$) or sequentially with 1 μM bryostatin-1 for 24 h followed by paclitaxel for 18 h (Bryo$_{24}$→T$_{18}$). The cells were harvested after paclitaxel therapy by trypsinization, pooled with floating cells, and fixed with 1% paraformaldehyde and 70% ethanol. After washing with PBS containing 0.05% Tween 20 and 1%

fetal bovine serum, cells were labeled with MPM-2 antibody (final concentration of 6 μg MPM-2 antibody/ml; Upstate Biotechnology, Lake Placid, NY) for 1 h at 4°C. Cells were washed twice with PBS and incubated with goat antimouse-FITC (Boehringer Mannheim, Mannheim, Germany) for 1 h at room temperature in the dark. After washing twice with PBS, cells were resuspended in 5 μg/ml propidium iodide containing 50 μg/ml RNase A. Samples were analyzed on a Becton Dickinson FACScan, and data were analyzed using CellQuest software. The MPM-2 positive cells (mitotic cells) will show increased green fluorescence, thus shifting above the baseline of the dot plot.

NMR. Proton-decoupled ^{31}P-NMR spectra were obtained from MCa tumors on the dorsal aspect of the foot of C3H mice at 81.03 MHz on a Bruker CSI 4.7T 33-cm horizontal bore magnet (Fremont, Ca). The unanesthetized mouse was suspended in an acrylic former with the leg immobilized and extended horizontally so that the tumor-bearing foot was surrounded by a 13-mm internal diameter four-turn teflon-coated solenoidal coil tuned to 81 MHz. Experimental parameters included a spectral width of 10,000 Hz, delay of 2 s, 60° flip angle, 4096 data points and 2048 free induction decays. The WALTZ-16 (Wonderful Alternating Phase technique for Zero Residual Splitting) routine was used to decouple during the acquisition. The free induction decays were zerofilled once, a double exponential multiplication filter of 6 was applied, and the transformed spectra were manually baseline-corrected. A single 13-mm internal diameter four-turn teflon-coated coil was used. Field homogeneity was improved, and temperature was maintained by immersing the tumor-bearing foot in a water bath at 37°C. Peak areas were estimated from the spectrum by fitting the spectra to a series of Lorentzian peaks while varying the peak position, height, and line-width to obtain the best fit using software available on the spectrometer (SPANTOOL). A decrease in the ratio of the PCr to Pi peak areas (PCr:Pi) is indicative of decrease energy status. Tumor pH is estimated from the chemical shift of the Pi resonance relative to PCr. Tumors were studied by NMR after attaining a volume of ~250 mm^3. Mice were treated with 160 μg/kg ($n = 4$), 120 μg/kg ($n = 4$), 80 μg/kg ($n = 8$),and 60 μg/kg ($n = 8$).

Tumor Perfusion. To analyze tumor perfusion, animals were studied using rapid MR imaging with Gd-DTPA contrast (Magnevist, Berlex Laboratories, Wayne, NJ). All of the studies were performed on a 4.7 Tesla Bruker-CSI imager with a 33-cm horizontal bore. Perfusion was studied 12 h after treatment with either 80 or 120 μg/kg of bryostatin-1 ($n = 7$ per group). To avoid the possibility of the remaining Gd-DTPA influencing the results, it was decided that baseline and posttreatment gadolinium studies should not be performed on the same mouse, although subsequent control experiments did not note any effect on signal intensity 12 h after injection of Gd-DTPA. A separate group of control animals with tumors in the same size range were used to provide baseline data. Tumor volumes ranged from 200 to 250 mm^3 for the perfusion studies.

In all of the perfusion studies, a 24-gauge i.v. catheter was introduced into the tail vein, and a syringe containing Gd-DTPA (0.02 ml diluted to a volume of 0.3 ml) was attached to the catheter. The unanesthetized mouse was suspended in an acrylic former with the leg immobilized and extended horizontally so

Table 1 LD10 of bryostatin-1

Dose	% mortality (7 days)	TDT (days)[a]
Saline	0 (0/5)	3.0 ± 0.3
Bryostatin 50 μg/kg	10 (1/10)	4.1 ± 0.3 (*P* < 0.05 compared with control)
Bryostatin 60 μg/kg	10 (1/10)	5.0 ± 0.7 (*P* < 0.05 compared with control)
Bryostatin 80 μg/kg	10 (1/10)	4.2 ± 0.3 (*P* < 0.01)
Bryostatin 100 μg/kg	40 (2/5)	6.9 ± 0.1[a] (*P* < 0.01 compared with 80 μg/kg)) (*P* < 0.0 compared with control)
Bryostatin 120 μg/kg	100 (4/4)	
Bryostatin 160 μg/kg	100 (5/5)	

[a] Based on mice that survived ≥7 days.

that the tumor-bearing foot was surrounded by a 2-turn, 1.5-cm-diameter solenoidal coil tuned to 200 MHz. Spin-lattice (*T1*)-weighted spin-echo scout images were acquired to localize the tumor and to prescribe the largest cross-sectional slice for dynamic imaging. A single 1.5-mm thick slice was imaged at high resolution [repeat interval (*TR*), 300 ms; echo time (*TE*), 10 ms; number of acquisitions (*NA*), 8; field of view (*FOV*), 40 mm; matrix, 256 × 128; voxel size, 0.156 × 0.3125 × 1.5 mm]. The same slice was then imaged dynamically using a spin-echo pulse sequence (*TR*, 100 ms; *TE*, 10 ms; *NA*, 2; 12.8 s per image; *FOV*, 40 mm; matrix, 64 × 64; voxel size, 0.62 × 0.62 × 1.5 mm). After 1 min, a bolus injection of Gd-DTPA was given, and imaging continued for 12.6 additional min.

After on-line reconstruction, data were exported to a Sun Ultra 1 workstation (Sun Microsystems, Mountain View, CA.) for analysis. In-house software was written to display and analyze the data using IDL 5.1 (Research Systems Inc., Boulder, CO.). For each tumor, the time course of signal intensity in three ROI was examined. These regions encompassed the center, the rim, or the entire tumor cross-section, respectively. The high resolution *T1*-weighted scout image was used for more accurate selection of ROI. Care was taken to avoid any contamination of the ROI due to the bones of the foot and normal adjacent tissue. For each ROI, the maximum slope and baseline intensity were determined. To search for the maximum slope, a five-point, 64-s, sliding window was applied to the first 3 min of the time-intensity curve (21). The window search method compensated for regional heterogeneity in the time point of initial uptake. The slope was determined by linear regression of the five time points within the window. The maximum slope within 2 min after injection of the contrast agent was found. The baseline value was calculated as the mean of the points prior to the maximum slope window. The maximum percent signal increase (SI_{max}) per unit time in the ROI was calculated according to the equation given below:

$$\%SI_{max} = \text{Maximum slope} * \frac{100}{SI_{pre}}$$

where the SI_{pre} value was the baseline average signal intensity. This equation represents a slight modification of the technique reported by Erlemann *et al.* (22). The identical algorithm was also applied to each voxel to generate parametric images of maximum percent signal intensity increase per unit time.

Statistical Analysis. All of the *in vitro* experiments were repeated at least three times unless otherwise indicated. The statistical significance of the animal studies was determined by the two-sided Student's *t* test from the mean ± SE.

RESULTS

Effect of Bryostatin-1 and Paclitaxel on Tumor Growth Delay. Table 1 shows the effect of different single doses of bryostatin-1 on tumor growth delay and survival. Bryostatin-1 as a single agent had modest activity in this tumor model. The maximum tolerated dose (LD10) for this tumor model was 80 μg/kg, for a single dose of bryostatin-1, which induced a TDT of 4.2 ± 0.3 days (*n* = 10), compared with 3.0 ± 0.3 days (*n* = 10) for untreated mice (*t* = 3.08; *P* < 0.01). Bryostatin-1 failed to show a dose response effect in the dose range of 50–80 μg/kg. The TDTs for mice treated with bryostatin-1 at both 50 and 60 μg/kg were also modestly greater than controls. A dose of 100 μg/kg induced a greater tumor growth delay for mice that survived the treatment. Nevertheless, this dose exceeded the acceptable mortality rate and was deemed toxic. Because 80 μg/kg of bryostatin-1 was the maximum tolerated dose in this tumor model, it was selected as the dose for the combination studies with paclitaxel.

The effect of treatment on tumor growth with the different drugs for three weekly cycles was evaluated. The effect of single agent bryostatin-1 could not be evaluated beyond 7–10 days because there was minimal tumor response and the tumors had grown to the point that the animals required sacrificing. The TDT after treatment with paclitaxel was 23.4 ± 1.7 days (*n* = 10). This is compatible with the drug's known activity in breast cancer (23). With bryostatin-1 followed by paclitaxel (bryostatin-1→paclitaxel), the TDT was decreased to 9.7 ± 1.1 days (*n* = 14), which indicated an antagonistic effect by bryostatin-1 on the paclitaxel-treated tumors. For mice that received the reverse combination of paclitaxel followed by bryostatin-1, the TDT was prolonged to 29.6 ± 0.6 days (*n* = 14; paclitaxel→bryostatin-1), which suggested an additive effect when compared with paclitaxel alone. The differences between paclitaxel, paclitaxel→bryostatin-1, and brytostatin-1→paclitaxel were all significant (*P* < 0.01). These *in vivo* data indicate that pretreatment with bryostatin-1 before paclitaxel will antagonize the effect of paclitaxel and emphasize that the interactions between bryostatin-1 and paclitaxel are sequence-dependent.

Effect of Bryostatin-1 on Paclitaxel-induced p34^{cdc2} Kinase Activity. One possible reason for the decreased response to the sequential bryostatin-1 followed-by-paclitaxel combination may be related to a cell cycle effect of bryostatin-1 on
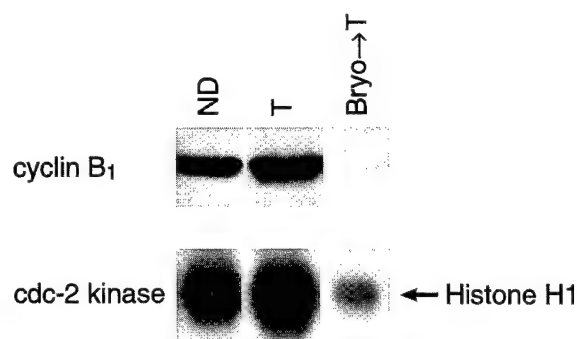
Fig. 1 Effect of sequential bryostatin-1 and paclitaxel on cyclin B_1 expression and p34^{cdc2} kinase activation. Mice bearing MCa tumors were treated with paclitaxel (*T*) or sequential bryostatin-1 followed by paclitaxel (*Bryo→T*) as described in "Materials and Methods." Tumor extracts were prepared, and protein levels were analyzed by immunoblotting for cyclin B_1. Using the Histone H1 kinase assay as described in "Materials and Methods," the kinase activity of p34^{cdc2} kinase was examined in the tumor extracts under identical conditions. Results from a representative experiment are shown.

paclitaxel-treated tumor cells. The effect of paclitaxel is dependent on metaphase arrest, which requires the activation of p34^{cdc2} kinase activity. p34^{cdc2} kinase activity is induced by its association with cyclin B_1 and dephosphorylation of cdc2 at Thr (14) and Tyr (15). Cyclin B_1 is induced in G_2 and continues to accumulate until metaphase (24, 25). We thus assayed cyclin B1-associated p34^{cdc2} kinase activity in the MCa tumor by histone H1 phosphorylation immediately after completing week 1 of therapy. As shown in Fig. 1, treatment with paclitaxel (*T*) alone resulted in a 20% increase in p34^{cdc2} kinase activity when compared with the untreated controls (*ND*). This was associated with a 60% increase in cyclin B_1 protein expression. However, with the treatment of bryostatin-1 followed by paclitaxel (*Bryo→T*), p34^{cdc2} kinase activity was decreased 10-fold, and cyclin B_1 protein expression was decreased 100-fold, compared with the untreated controls. This would indicate that pretreatment with bryostatin-1 prevents the activation of p34^{cdc2} kinase, a cell cycle event that is critical for paclitaxel's anticancer effect.

Effect of Bryostatin-1 on Mitotic Entry of Paclitaxel-treated Gastric Cancer Cells. Because bryostatin-1 prevents p34^{cdc2} kinase activation by paclitaxel, we evaluated the effect of bryostatin-1 on paclitaxel-induced mitotic entry. This is difficult to evaluate *in vivo*, and, therefore we elected to examine the effect of sequential bryostatin-1 followed by paclitaxel therapy *in vitro* in MKN-74 gastric cancer cells. The percentage of mitotic cells was determined by MPM-2 labeling. MPM-2 antibody recognizes epitopes shared by phosphoproteins that appear during mitosis (26). Two-dimensional flow cytometry was used to quantitate the population of cells in M phase. As shown in Table 2, in untreated cells (No drug) only 2% of the cells stain positively for MPM-2. However, with paclitaxel treatment alone for 18 h (T_{18}), 56% of the cells stain positively for MPM-2, consistent with mitotic entry. In contrast, pretreatment of MKN-74 cells with bryostatin-1 for 24 h before paclitaxel ($Bryo_{24} \rightarrow T_{18}$) resulted in only 23% of the cells staining positively for MPM-2. This would suggest that pretreatment of cells

Table 2 Effect of sequential bryostatin-1 and paclitaxel on mitotic arrest

MKN-74 cells were treated with paclitaxel for 18 h (T_{18}), bryostatin-1 for 24 h ($Bryo_{24}$), bryostatin-1 for 24 h followed by paclitaxel for 18 h ($Bryo_{24} \rightarrow T_{18}$), and paclitaxel for 18 h followed by bryostatin-1 for 24 h ($T_{18} \rightarrow Bryo_{24}$). Cells were labeled with the MPM-2 antibody and analyzed by flow cytometry for cells in mitosis, as described in "Materials and Methods." Results from a representative experiment are shown.

Conditions	G_1 (%)	S phase (%)	G_2 (%)	M (%)
No drug	34	47	17	2
T_{18}	10	13	21	56
$Bryo_{24}$	65	15	17	3
$Bryo_{24} \rightarrow T_{18}$	22	28	27	23
$T_{18} \rightarrow Bryo_{24}$	9	18	69	4

with bryostatin-1 before paclitaxel prevented the cells from entering into mitosis. Prevention of entry into mitosis by pretreatment with bryostatin-1 also antagonizes the effect of paclitaxel in these cells (data not shown). With the reverse sequence of $T_{18} \rightarrow Bryo_{24}$, the cells that had entered the M phase with paclitaxel alone (56%) have clearly exited M (4%) after 24 h of additional bryostatin-1 therapy. Interestingly, bryostatin-1 treatment alone causes an accumulation of cells in G_1.

Effect of Bryostatin-1 on Intratumoral Energy and pH. Because energy metabolism has been shown to be involved in apoptosis [although it remains controversial whether this represents a cause or effect (27)], and bryostatin-1 has been reported to change energy metabolism in muscle, we evaluated the effect of bryostatin-1 on intratumoral energy and pH by NMR. Fig. 2 shows a series of ^{31}P-NMR spectra obtained before and after bryostatin-1 at multiple time points after 80 (Fig. 2A) and 60 μg/kg (Fig. 2B) of bryostatin-1. The spectra showed peaks arising from the phosphomonoesters [phosphoethanolamine (*peaks A*) and phosphocholine (*peaks B*)], Pi (*peaks C*), phosphodiesters [glycerophosphoethanolamine (*peaks D*), and glycerophosphocholine (*peaks E*)], PCr (*peaks F*), and nucleoside triphosphates [γNTP (*peaks G*), αNTP (*peaks H*), NAD(H) (*peaks I*), βNTP (*peaks J*)]. As expected, the peaks are well resolved, which facilitates quantitation. At 12 h after treatment with bryostatin-1, a reduction in the peak areas of PCr:Pi was noted. Fig. 3 shows the changes in PCr:Pi and pH noted after the treatment of eight tumor-bearing mice with bryostatin-1 at a dose of 80 μg/kg. A decrease in PCr:Pi at 12 h was statistically significant ($P < 0.03$). This indicates a loss of high-energy phosphate (PCr) and an increase in free Pi and is consistent with a decrease in intratumoral energy. This effect persisted up to 40 h after bryostatin-1 therapy. Depletion in energy at 12 h after 120 μg/kg ($n = 4$ animals; data not shown) was greater than after 80 μg/kg, although the differences did not attain significance ($P < 0.10$). After treatment with 80 μg/kg of bryostatin-1, there is a maximum drop of 0.13 ± 0.02 pH units noted at 12 h posttreatment, which shows recovery by 48 h. It is noted that, after treatment with bryostatin-1, the Pi peak (*peak C*) shifts upfield, which is indicative of tumor acidosis, compared with the pretreatment pH. As shown in Fig. 2, the Pi peak was also often split into multiple resonances indicative of pH heterogeneity in the tumor.
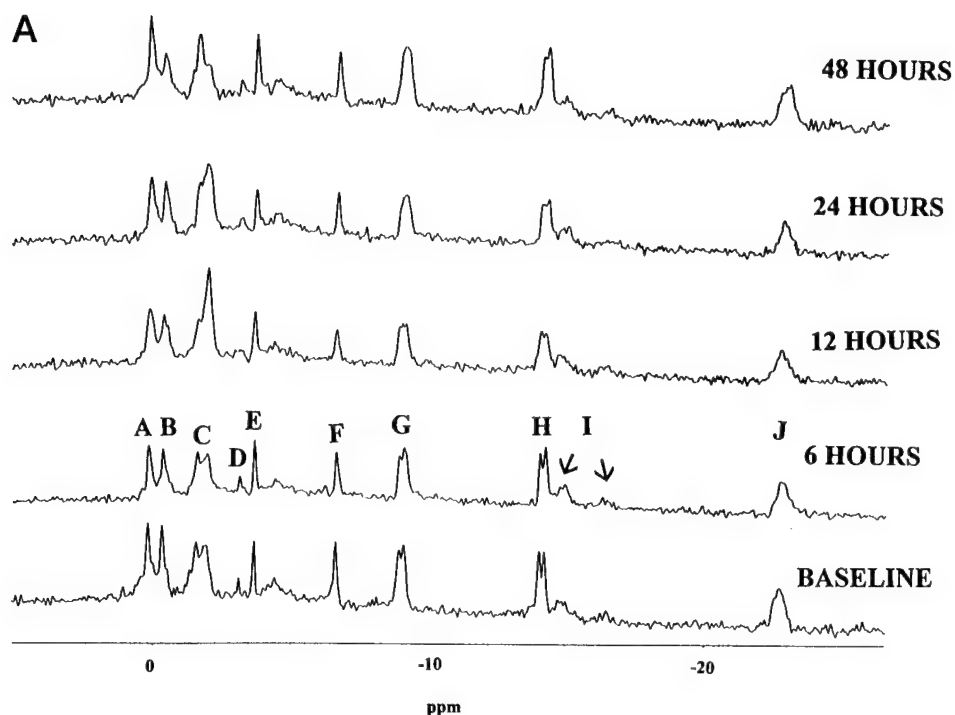
Fig. 2 A, ^{31}P-NMR spectra obtained before and after 80 µg/kg bryostatin-1. Peaks include A, phosphoethanolamine; B, PC; C, Pi; D, glycerophosphoethanolamine; E, glycerophosphocholine; F, PCr; G, γNTP; H, αNTP; I, NAD(H); and J, βNTP. The Pi peak shifts upfield (*to the right*) after treatment, which is indicative of a decrease in pH. *B*, ^{31}P-NMR spectra obtained before and after 60 µg/kg byostatin-1. There is a decrease in PCr peak relative to the Pi peak after treatment with bryostatin-1.
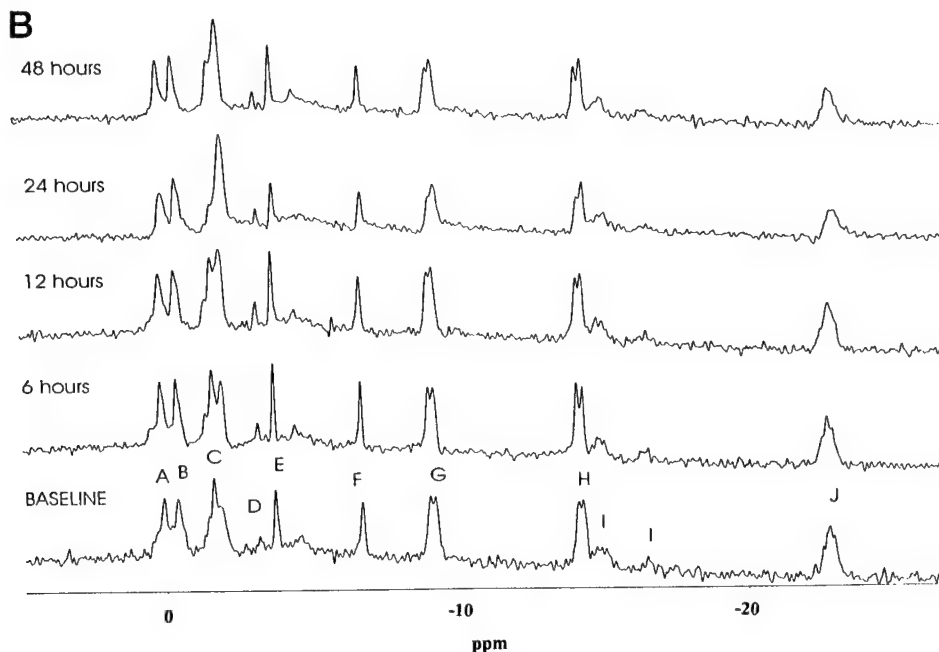
Effect of Bryostatin-1 on Tumor Blood Flow. Another possible reason for decreased response (when mice were treated initially with bryostatin-1 followed by paclitaxel) was decreased drug delivery or changes in the tumor microenvironment secondary to decreased tumor blood flow. Previous studies (28, 29) have indicated that the initial rate of uptake of Gd-DTPA is related to perfusion. Therefore, to analyze tumor perfusion, animals were studied using rapid MR imaging with Gd-DTPA

12 h after treatment with 80 µg/kg of bryostatin-1 ($n = 7$). The average signal-intensity-enhancement time-course curve for control animals, and for mice treated with 80 µg/kg of bryostatin-1, is shown in Fig. 4. There is a slower rate of rise of the signal in both the middle part of the tumor and particularly the rim after bryostatin-1. Similarly, there is a decrease in the maximum signal intensity attained. In Table 3, the maximum percent signal enhancement and maximum slope are shown
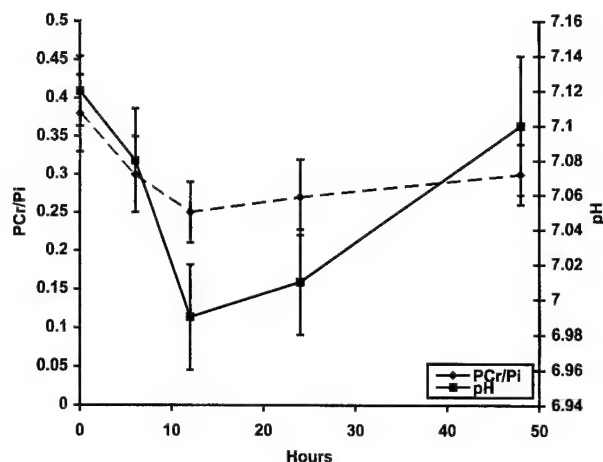
Fig. 3 Changes in PCr:Pi (*PCr/Pi*) and pH after treatment with bryostatin-1 at 80 μg/kg. Changes at 12 h were significant.

for control mice and tumor-bearing mice treated with 80 μg/kg of bryostatin-1. A significant reduction in the slope of the plot of signal intensity *versus* time was seen at bryostatin-1 doses of 80 μg/kg in the rim area ($P < 0.005$), which suggests a decrease in tumor perfusion in the rim of the tumor. Changes in the central region of the tumor were not significantly different after bryostatin-1 ($P = 0.20$). Averaging the result over the whole tumor volume indicated that bryostatin-1 did induce a change in the maximum slope ($P < 0.03$). Control studies indicated that the effect of paclitaxel on perfusion in the rim of the tumor approached, but did not attain, statistical significance ($P < 0.08$).

DISCUSSION

We have investigated the effect of bryostatin-1 in combination with paclitaxel on tumor growth and on paclitaxel-induced p34^{cdc2} kinase activity, mitotic entry, tumor metabolism, and perfusion. This is the first *in vivo* data to indicate that pretreatment with bryostatin-1 decreases the efficacy of paclitaxel, whereas the reverse sequence (paclitaxel→bryostatin-1) shows a statistically significant increase in efficacy compared with single-agent paclitaxel. Therefore, in contrast to other drug combinations, pretreatment with bryostatin-1 will antagonize rather than enhance the paclitaxel effect. Our results indicate that, in mouse mammary tumors, bryostatin-1 blocks the activation of p34^{cdc2} kinase activity in association with a decrease in the protein expression of the p34^{cdc2} kinase activator, cyclin B_1. The anticipated effect of this on the cell cycle of these mouse mammary tumors is to decrease the percentage of cells entering mitosis when treated with paclitaxel. MCa tumors grow only *in vivo* and are not amenable to *in vitro* analysis by flow cytometry. Using the MKN-74 gastric cancer cell line, we were able to show by flow cytometry that the treatment of tumor cells with bryostatin-1 before paclitaxel decreases mitotic entry. In addition, *in vivo* NMR studies indicate that bryostatin-1 induces a decrease in intratumoral energy, pH, and blood flow that may adversely affect the efficacy of subsequent paclitaxel therapy.

To investigate the reason for the decreased efficacy of

paclitaxel after treatment with bryostatin-1, we first investigated the effect of bryostatin-1 on mitotic events that pertain to paclitaxel. Paclitaxel is a mitotic spindle inhibitor and induces mitotic block in a variety of cell lines (30). The critical events associated with paclitaxel-induced apoptosis are not known; however, it has been shown that mitotic block induces apoptosis by stabilizing microtubule dynamics rather than by alteration of the microtubule mass (31). The importance of mitotic block in inducing apoptosis in response to paclitaxel has also been shown by various groups using antisense of cyclin B_1 to abrogate the p34^{cdc2} kinase activity (32). The prevention of mitotic block also prevents the cell death. Therefore, we elected to explore whether there were cell cycle events relative to p34^{cdc2} kinase activity that could explain the lack of tumor response relative to the sequential bryostatin-1 followed by paclitaxel therapy. Analysis of the tumor tissues shows that bryostatin-1 inhibits p34^{cdc2} kinase activity in association with a decrease in the expression of cyclin B_1 protein, the p34^{cdc2} kinase activator.

Further examination of this event in an *in vitro* system also indicated that bryostatin-1 pretreatment prevents entry of tumor cells into mitosis by paclitaxel. Because mitotic entry is critical for the paclitaxel effect, these results indicate that the timing of bryostatin-1 relative to paclitaxel will inhibit the activation of p34^{cdc2} kinase activity by paclitaxel, inhibit mitotic entry, and antagonize the paclitaxel effect. Although the latter study was done in a different tumor model, it still supports the hypothesis that pretreatment of tumor cells with bryostatin-1 will block the effect of paclitaxel.

These studies do not exclude the importance of other cell cycle events in this process. For example, Asiedu *et al.* (5) has reported *in vitro* that bryostatin-1 induces p21 in U937 leukemic cells and inhibits CDK2 activity. These events are capable of inducing a G_1 arrest, which could also prevent paclitaxel treated cells from entering the M phase of the cell cycle, thus antagonizing the paclitaxel effect. This may, in fact, explain the increase in the G_1 population observed in the MKN-74 cells after treatment with single-agent bryostatin-1. Wang *et al.* (18) has reported *in vitro* an increase in the induction of apoptosis of U937 human leukemic cells when bryostatin-1 was given after, not before, paclitaxel. They attribute this effect, in part, to an increase in the amount of free Bax, a proapoptotic protein that is not detected in our cells. However, we could not detect changes in the bax:bcl-2 ratio, nor could we detect an increase in p21 in our tumor cells (data not shown). Nevertheless, with the bryostatin-1/paclitaxel combination, there seems to be a sequential dependency that depends on an ordering of events relative to cell cycle effect.

Hickman *et al.* (9) and Thompson *et al.* (10), in previous studies, demonstrated that bryostatin-1 induces changes in muscle metabolism. Specifically, they noted a significant increase in the phosphodiester:ATP ratio at 48 h after bryostatin-1 treatment, which suggests a decrease in high-energy phosphates. This could result in antagonism of the subsequent paclitaxel effect. Hydrolysis of high-energy phosphates, especially GTP, has been shown to play an important role in paclitaxel-induced microtubule assembly (33, 34). Thus, the decrease in high-energy phosphates induced by bryostatin-1 *in vivo* could result in impaired tubulin polymerization by subsequent paclitaxel therapy.
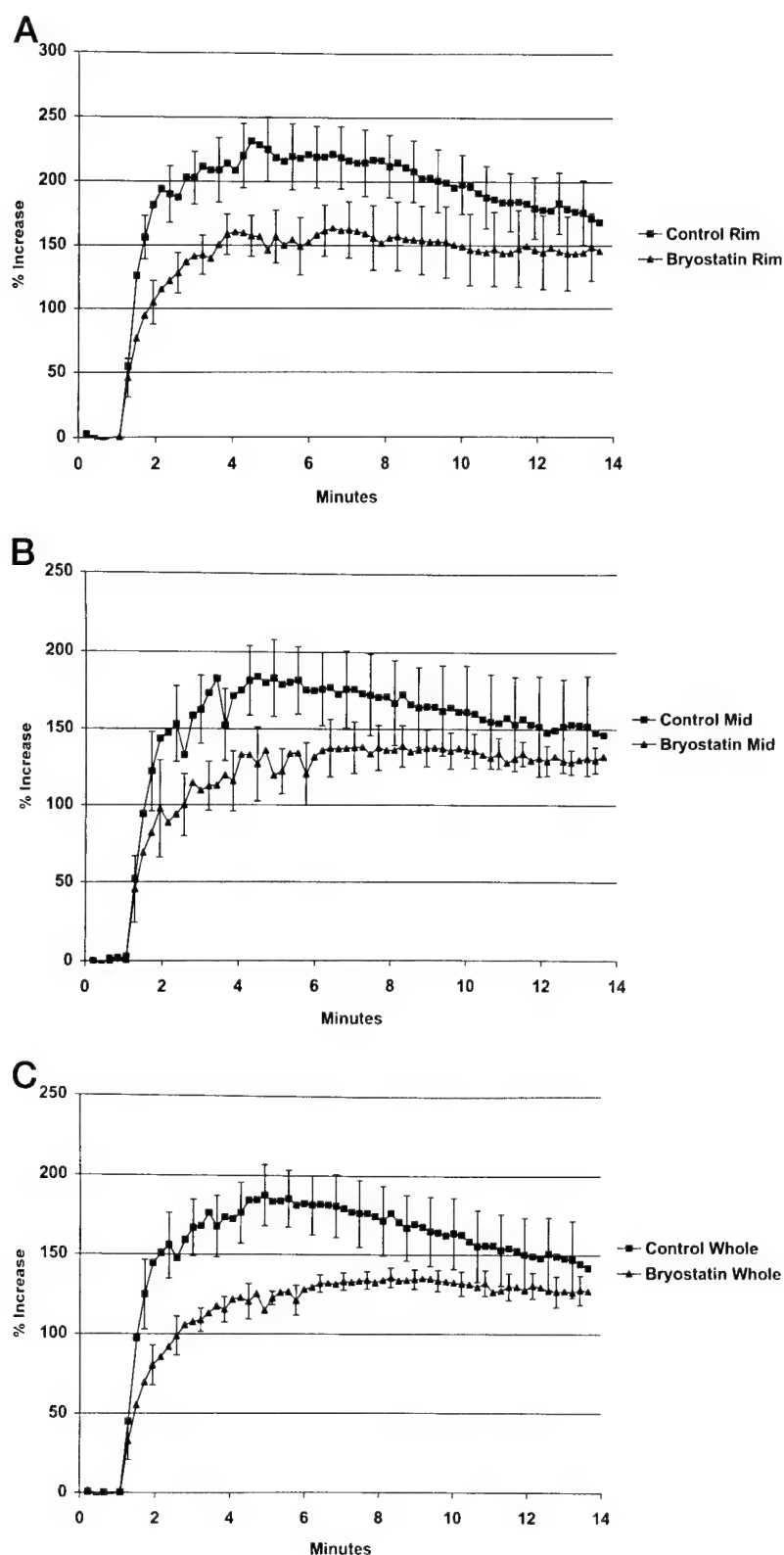
Fig. 4 Percent change in tumor signal intensity after a dose of Gd-DTPA in control tumor-bearing mice or 12 h after the tumor-bearing mice were treated with bryostatin-1. *A*, rim of tumor; *B*, central core of tumor; *C*, whole tumor. There were modest differences in the center and rim of the tumor between control and tumor-bearing mice treated with bryostatin-1, which approached significance. The change in maximum enhancement over the whole tumor was significant ($P = 0.05$).

Hickman *et al.* (9) also noted a decrease in the proton efflux rate at 4 h after bryostatin-1, which indicated a decrease in muscle blood flow. In three of four patients studied with near IR spectroscopy, they found a reduced rate of postexercise reoxygenation that was consistent with reduced blood flow. This was associated with impaired mitochondrial energy production,

Table 3 Effect of bryostatin-1 on the rate of Gd-DTPA uptake and signal intensity

	Control ($n = 6$)	80 µg/kg ($n = 7$)
Maximum slope		
Rim	230.8 ± 15.9	127.6 ± 20.1[a]
Center	166.9 ± 27.6	116.9 ± 37.0
Whole tumor	168.1 ± 23.1	93.8 ± 10.8[b]
Maximum % increase in intensity		
Rim	246.3 ± 22.8	187.5 ± 20.8
Center	218.4 ± 24.6	159.3 ± 19.2
Whole tumor	202.6 ± 21.6	145.2 ± 7.7

[a] $P < 0.005$ compared with control cohort.

[b] $P < 0.03$ compared with control.

which was consistent with either vasoconstriction or direct mitochondrial toxicity. Additional studies were carried out attempting to reverse the myalgias, induced by bryostatin-1, by treatment with nifedipine. They concluded that bryostatin-1 likely did induce vasoconstriction but that it was not the cause of the bryostain-1-induced myalgias.

The mouse mammary carcinoma perfusion studies, although not proving cause, indicated that tumor perfusion decreased after bryostatin-1. This in itself could explain the decrease in pH and PCr:Pi. In nearly all of the tumor-bearing animals treated with 80 µg/kg of bryostatin-1 (seven of eight), splitting of the Pi peak (or enhanced splitting compared with pretreatment) was detected within the first 24 h of treatment, which indicated a greater heterogeneity of tumor pH favoring acidosis. This suggested that the effect induced by bryostatin-1 on the tumor was not uniform. This is also more suggestive of an effect on blood flow, as opposed to an inhibition of a biochemical process, because tumor blood flow is typically heterogeneous. This heterogeneity is further confirmed by the perfusion studies, which showed variation over the image in the parametric plots of changes in signal over time.

This decrease in tumor blood flow by bryostatin-1 may explain the slight increase in TDT with bryostatin-1 as a single agent. This also may result in a decrease in drug delivery of subsequent paclitaxel therapy to the tumor site. Additional studies with a NMR-visible drug (5-fluorouracil) are under way to determine whether bryostatin-1 decreases drug delivery to the tumor; this would corroborate the hypothesis that the inhibition of cell kill after pretreatment with bryostatin-1 is in part due to decreases in perfusion.

Treatment with bryostatin-1 induced a decrease in tumor pH. Previous studies (35–37) have demonstrated that small decreases in pH can increase the induction of apoptosis. This would suggest that pretreatment with bryostatin-1 might enhance, rather than antagonize, the effect of paclitaxel. However, this was not the case in our model system. One possibility for this is that the cytotoxicity of paclitaxel is decreased at a reduced pH (38). A decrease in pH has also been associated with increased accumulation of cells in the G_1 phase of the cell cycle, in which they are more resistant to the effect of the drug (38).

The dynamic ordering of events seems to be of critical importance, as the combination of paclitaxel and bryostatin-1 enters clinical trials. Alterations in particular events associated with the interactions between these two drugs, especially the effects on energy metabolism and blood flow, could only have been detected in an *in vivo* system. On the basis of these laboratory studies, we have launched a Phase I clinical trial of weekly sequential paclitaxel and bryostatin-1 (39). On the basis of our preclinical models, patients are treated for at least 3 weeks with a fixed dose of paclitaxel on day 1 followed by bryostatin-1 at escalating doses in each cohort on day 2 of the weekly therapy. In this clinical trial, we have not observed any changes in paclitaxel pharmacokinetics, even with increasing doses of bryostatin-1. Although paclitaxel pharmacokinetics were not studied in the animals, these clinical results would suggest that a change in paclitaxel pharmacokinetics by bryostatin-1 would not account for the antagonism or enhancement observed with bryostatin-1 on the paclitaxel-treated mouse mammary tumors. Also, there are currently no available methods to measure bryostatin-1 levels in the plasma. Therefore, it is not possible to determine whether the doses of bryostatin-1 that we are using in the animals are comparable to those that are achievable in patients. To date, we have observed clinical activity with manageable toxicity in patients with recurrent esophagus and pancreatic cancer. These exciting clinical results represent a new direction in cancer therapy and illustrate the importance of the cell cycle, energy metabolism, and blood flow in the development of bryostatin-1 for clinical trials.

REFERENCES

1. Hornung, R. L., Pearson, J. W., Bechwith, M., and Longo, D. L. Preclinical evaluation of bryostatin-1 as an anticancer agent against several murine tumor cell lines: *in vitro versus in vivo* activity. Cancer Res., *52:* 101–107, 1992.

2. Schucter, L. M., Esa, A. H., and May, W. S. Successful treatment of murine melanoma with bryostatin-1. Cancer Res., *51:* 682–687, 1991.

3. Stanwell, C., Geischer, A., Bradshaw, T. D., and Petit, G. R. The role of protein kinase C isoenzymes in human inhibition caused by bryostatin-1 in human A549 lung and MCF-7 breast carcinoma cells. Int. J. Cancer, *56:* 585–592, 1994.

4. Hennings, H., Blumberg, P. M., Petit, P. M., Herald, C. L., Shores, R., and Yuspa, S. Bryostatin-1, activator of protein kinase C inhibits, tumor promotion by phorbol esters in sencar mouse skin. Carcinogenesis (Lond.), *9:* 1343–1346, 1987.

5. Asiedu, C., Biggs, J., Lilly, M., and Kraft, A. S. Inhibition of leukemic cell growth by the protein kinase C activator bryostatin 1 correlates with the dephosphorylation of cyclin dependent kinase 2. Cancer Res., *55:* 3716–3720, 1995.

6. Szallasi, Z., Linh, D., Levine, R., Lewin, N. E., Nguyen, P. N., Williams, M. D., Pettit, G. R., and Blumberg, P. M. The bryostatins inhibit growth of B16/F10 melanoma cells *in vitro* through a protein kinase C-independent mechanism: dissociation of activities using 26-epi-bryostatin 1. Cancer Res., *56:* 2105–2111, 1996.

7. Philip, P. A., Rea, D., Thavasu, P., Carmichael, J., Nicholas, S. A., Rockett, H., Talbot, D. C., Ganesman, T., Petit, G. R., Balkwill, F., and Harris, A. L. Phase I study of bryostatin 1: assessment of interleukin 6 and tumor necrosis factor α induction *in vivo*. J. Natl. Cancer Inst., *85:* 1812–1818, 1993.

8. Mohr, H., Pettit, G. R., and Plessing-Menze, A. Co-induction of lymphokine synthesis by the antineoplastic bryostatins. Immunobiology, *175:* 420–430, 1987.

9. Hickman, P. F., Kemp, G. J., Thompson, C. H., Salisbury, A. J., Wade, K., Harris, A. L., and Radda, G. K. Bryostatin-1, a novel antineoplastic agent and protein kinase C activator induces human myalgia and muscle metabolic defects: a 31P magnetic resonance spectroscopic study. Br. J. Cancer, *72:* 998–1003, 1995.

10. Thompson, C. H., Macauleay, V. M., O'Byrne, K. J., Kemp, G. J., Wilner, S. M., Talbot, D. C., Harris, A. L., and Radda, G. K. Modulation of bryostatin-1 toxicity by nifedipine: effects on muscle metabolism and oxygen supply. Br. J. Cancer, *73:* 1161–1164, 1996.

11. Jayson, G. C., Crowther, D., Prendiville, J., McGowan, A. T., Scheid, C., Stern, P., Young, R., Brenchley, P., Chang, J., Owens, S., and Pettit, G. R. A Phase I trial of bryostatin-1 in patients with advanced malignancy using a 24-hour intravenous infusion. Br. J. Cancer, *72:* 461–468, 1995.

12. Prendiville, J., Crowther, D., Thatcher, N., Woll, P. J., Fox, B. W., McGowan, A., Testa, N., Stern, P., McDermott, R., Potter, M., and Pettit, G. R. A Phase I study of intravenous bryostatin-1 in patients with advanced cancer. Br. J. Cancer, *68:* 418–424, 1993.

13. Grant, S., Roberts, J., Poplin, E., Tombes, M. B., Kyle, B., Welch, D., Carr, M., and Bear, H. D. Phase Ib trial of bryostatin-1 in patients with refractory malignancies. Clin. Cancer Res., *4:* 611–618, 1998.

14. Jarvis, W. D., Povirk, L. F., Turner, A. J., Traylor, R. S., Gewirtz, D. A., Pettit, G. R., and Grant, S. Effects of bryostatin-1 and other pharmacological activators of protein kinase C on 1-β-D-arabinofurano-sylcytosine-induced apoptosis in HL-60 human promyelocytic leukemia cells. Biochem. Pharmacol., *47:* 839–852, 1994.

15. Mohammad, R. M., Diwakaran, H., Maki, A., Emarra, M. A., Pettit, G. R., Redman, B., and al-Katib, A. Bryostatin-1 induces apoptosis and augments inhibitory effects of vincristine in human diffuse large cell lymphoma. Leuk. Res., *19:* 667–673, 1995.

16. Mohammad, R. M., al-Katib, A., Pettit, G. R., and Sensenbrenner, L. L. Successful treatment of human Waldenstrom's macroglobulinemia with combination biological and chemotherapy agents. Cancer Res., *54:* 165–168, 1994.

17. Basu, A, and Lazo, J. S. Sensitization of human cervical carcinoma cells to cis-diamminedichloroplatinum (II) by bryostatin-1. Cancer Res., *52:* 3119–3124, 1992.

18. Wang, S., Guo, C. Y., Castillo, A., Dent, P., and Grant, S. Effect of bryostatin-1 on Taxol-induced apoptosis and cytotoxicity in human leukemia cells (U937). Biochem. Pharmacol., *56:* 635–644, 1998.

19. Motwani, M., Delohery, T. M., and Schwartz, G. K. Sequential dependent enhancement of caspase activation and apoptosis by flavopiridol on paclitaxel-treated human gastric and breast cancer cells. Clin. Cancer Res., *5:* 1876–1883, 1999.

20. Koutcher, J. A., Alfieri, A. A., Devitt, M. L., Rhee, J. G., Kornblith, A. B., Mahmood, U., Merchant, T. E., and Cowburn, D. Quantitative changes in tumor metabolism, partial pressure of oxygen, and radiobiological oxygenation status postradiation. Cancer Res., *52:* 4620–4627, 1992.

21. Reddick, W., Langston, J., Meyer, W., Gronemeyer, S., Steen, R., Chen, G., and Taylor, J. Discrete signal processing of dynamic contrast-enhanced MR imaging: statistical validation and preliminary clinical application. J. Magn. Reson. Imaging, *4:* 397–404, 1994.

22. Erlemann, R., Sciuk, J., Bosse, A., Ritter, J., Kusnierz-Glaz, C., Peters, P., and Wuisman, P. Response of osteosarcoma and Ewing sarcoma to preoperative chemotherapy: assessment with dynamic and static MR imaging and skeletal scintigraphy. Radiology, *175:* 791–796, 1990.

23. Seidman, A. D., Hudis, C. A., Raptis, G., Baselga, J., Fennelly, D., and Norton, L. Paclitaxel for breast cancer: the Memorial Sloan-Kettering Cancer Center experience. Oncology (Huntingt.), *11* (Suppl. 2)*:* 20–28, 1997.

24. Poon, R. Y. C., Chau, M. S., Yamashita, K., and Hunter, T. The role of Cdc2 feedback loop control in the DNA damage checkpoint in mammalian cells. Cancer Res., *57:* 5168–5178, 1997.

25. Nurse, P. Universal control mechanism regulating onset of M-phase. Nature (Lond.), *344:* 503–508, 1990.

26. Vandre, D. D., and Borisy, G. G. Anaphase onset and dephosphorylation of mitotic phosphoproteins occur concomitantly. J. Cell Sci., *94:* 245–258, 1989.

27. Martin, D. S., and Schwartz, G. K. Chemotherapeutically induced DNA damage, ATP depletion, and the apoptotic biochemical cascade. Oncol. Res., *9:* 1–5, 1997.

28. Belfi, C. A., Ting, L. L., Hassenbusch, S. J., Tefft, M., and Ngo, F. Q. H. Determination of changes in tumor blood perfusion after hydralazine treatment by dynamic paramagnetic-enhanced magnetic resonance imaging. Int. J. Radiat. Oncol. Biol. Phys., *22:* 477–482, 1992.

29. Kennedy, S. D., Szczepaniak, L. S., Gibson, S. L., Hilf, R., Foster, T. H., and Bryant, R. G. Quantitative MRI of Gd-DTPA uptake in tumors: response to photodynamic therapy. Magn. Reson. Med., *31:* 292–301, 1994.

30. Schiff, P. B., and Horwitz, S. B. Taxol stabilizes microtubules in mouse fibroblast cells. Proc. Natl. Acad. Sci. USA, *77:* 1561–1565, 1980.

31. Jordan, M. A., Wendell, K., Gardiner, S., Derr, W. B., Copp, H., and Wilson, L. Mitotic block induced in Hela cells by low concentrations of paclitaxel (Taxol) results in abnormal mitotic exit and apoptotic cell death. Cancer Res., *56:* 816–825, 1996.

32. Shen, S., Huang, J. S., and Kuo, M. Taxol-induced p34^{cdc2} kinase activation and apoptosis inhibited by 12-O-tetradecanoylphorbol-13-acetate in human breast MCF-7 carcinoma cells. Cell Growth Differ., *9:* 23–29, 1998.

33. Carlier, M. F., and Pantaloni, D. Taxol effect on tubulin polymerization and associated guanosine 5'-^{8}triphosphate hydrolysis. Biochemistry, *22:* 4814–4822, 1983.

34. Vulevic, B., and Correia, J. J. Thermodynamic and structural analysis of microtubule assembly: role of GTP hydrolysis. Biophys. J., *72:* 1357–1375, 1997.

35. Reynolds, J. E., Li, J., Craig, R. W., and Eastman, A. BCL-2 and MCL-1 expression in Chinese hamster ovary cells inhibits intracellular acidification and apoptosis induced by staurosporine. Exp. Cell Res., *225:* 430–436, 1996.

36. Chen, Q., Benson, R. S. P., Whetton, A. D., Brant, S. R., Donowitz, M., Montrose, M. H., Dive, C., and Watson, A. J. M. Role of acid/base homeostasis in the suppression of apoptosis in haemopoietic cells by v-Abl protein tyrosine kinase. J. Cell Sci., *110:* 379–387, 1997.

37. Gottlieb, R. A., Nordberg, J., Skowronski, E., and Babior, B. M. Apoptosis induced in Jurkat cells by several agents is preceded by intracellular acidification. Proc. Natl. Acad. Sci. USA, *93:* 654–658, 1996.

38. Vukovic, V., and Tannock, I. F. Influence of low pH on cytotoxicity of paclitaxel, mitoxantrone, and topotecan. Br. J. Cancer, *75:* 1167–1172, 1997.

39. Kaubisch, A., Kelsen, D. R., Saltz, L., Kemeny, N., O'Reilly, E., Ilson, D., Endres, S., Barazzuol, J., and Schwartz, G. K. A Phase I trial of weekly sequential bryostatin-1 and paclitaxel in patients with advanced solid tumors. Proc. Am. Soc. Clin. Oncol., *18:* 166a, 1999.

Effect of 6-Aminonicotinamide on Human Tumor Metabolism, and Response to Chemotherapy and Radiation

Anne Holleran*, Yuchun Chen, and Jason A. Koutcher
US Patent Office* and Memorial Sloan Kettering Cancer Center

Introduction

Previous studies from different investigators (1,2) have indicated that 6-aminonicotinamide (6AN) can enhance anti-neoplastic treatment. In a previous study of RIF-1 cells, the surviving fraction after radiation was decreased if the cells were pretreated with 6AN (1). We have investigated the effect of 6AN on survival of human mammary tumor cells (MCF-7) after treatment with radiation, adriamycin and paclitaxel.

Methods

Cells – NMR – MCF-7 cells were grown on Culti-spher gelatin beads in media consisting of 50% DMEM and 50% minimal essential media with 10% FBS. Cells ($1-2 \times 10^7$) were mixed with 0.2 g beads in 50 ml media in a spinner flask for 18-24 hours without stirring. They were subsequently stirred for about 4-6 days at 30-40 rpm. Experiments were started when greater than 90% of the beads were greater than 50% covered with cells.

Cells – cytotoxicity studies – 1.3×10^5 cells were subcultured for 4 days and subsequently exposed to 6AN for 4 hours. 6AN containing media was replaced with fresh media and 3 hours later the cells were exposed to radiation (2,3,or 4 Gy), adriamycin (4 hours) or paclitaxel (24 hours). Subsequently, the cells were trypsinized and counted using a Coulter Counter. After radiation, cells were returned to the incubator for 3 hours of recovery and then trypsinized and counted.

NMR – MCF-7 cells grown on collagen beads were placed in a 12 mm shortened screw cap NMR tube which was connected to a perfusate reservoir via tubing. The pumping speed was adjusted so that the beads floated to the beginning of the widest cross-sectional area of the tube, about a cm from the top. NMR spectra were collected using a 5 turn solenoid coil wrapped around the 12 mm NMR tube. WALTZ decoupled 31P spectra were obtained using a 4.7T Bruker Omega CSI system operating at 81.03 MHz. Spectra were obtained prior to perfusion with 6AN, during the 4 hours of 6AN exposure (200uM) and subsequently after washout of 6AN for about 24 hours. Each spectrum required about 70 minutes to acquire.

Results

Figure 1 shows a series of spectra obtained on perfused MCF-7 cells. The peaks detected prior to 6AN perfusion include phosphoethanolamine (PE) (B), phosphocholine (PC) (C), inorganic phosphate (Pi) (D), glycerophosphoethanolamine (GPC) (E), glycerophosphocholine (GPC) (F), phosphocreatine (PCr) (G), γ, α and β NTP (peaks H,I and L), and diphosphodiesters (DPDE) (peaks J and K). The Pi peak was usually split into two components after treatment with 6AN which likely represented resolution of intra- and extra-cellular pH. During the infusion of 6AN and subsequently, a peak previously assigned to 6-phosphogluconate (6PG) was detected (A). As in studies with the RIF-1, this was the dominant peak in the spectrum and was visible for >24 hours post washout of 6AN. The baseline spectrum in Fig. 1 requried 70 minutes while subsequent spectra required 135 minutes of data acquisition.

The effect of 4 Gy of radiation was significantly enhanced by pretreatment with 6AN. The surviving fraction (SF) after 4 Gy was 0.087 ± 0.007 compared to 0.036 ± 0.018 for cells exposed to 6AN before radiation. 6AN alone had no effect on SF; similarly radiation followed by 6AN did not show an enhanced effect.

Pretreatment with 6AN (200uM) resulted in an enhanced efficacy of adriamycin at low concentrations (10^{-8} M), but this effect was lost at higher concentrations. This may be due to the very low cell survival that was present at higher doses of adriamycin. Pretreatment with 6AN followed by paclitaxel failed to show any enhancement. The activity of paclitaxel is dependent on cells traversing mitosis and therefore further studies to determine if 6AN may inhibit cells from entering mitosis are ongoing.

The current study corroborates a previous study (1) which showed enhancement of the effect of radiation by 6AN. The previous study was done in a murine tumor cell line, whereas this study demonstrates radiation enhancement in a human tumor cell line. Furthermore, this study also shows enhancement with adriamycin, one of the two most active agents used in breast cancer. Since adriamycin has a risk of cardiac toxicity at higher doses, it may be feasible by adding 6AN to achieve equi-efficacious activity with a lower dose of adriamycin, thereby decreasing the risk of cardiac toxicity.

References

1. Street et al J. Biol. Chem, 271, 4113, 1996
2. Budihardjo II et al Clin Cancer Res. 117, 1998
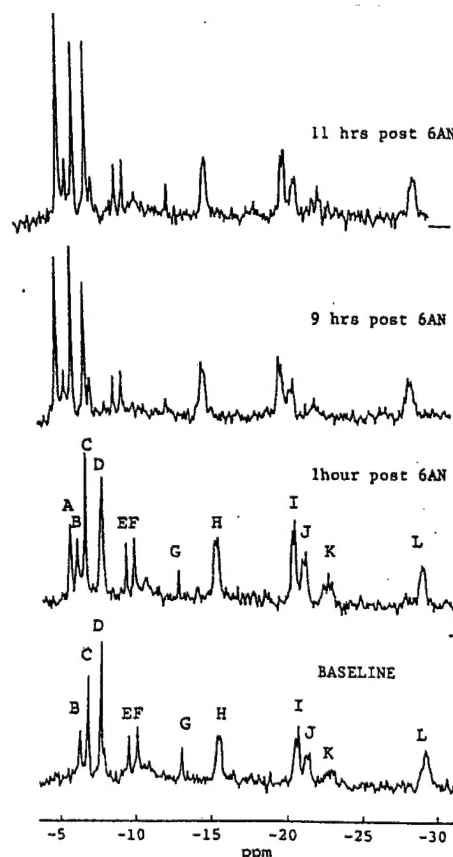
cally proved intrathoracic lymphoproliferative disorder and positive testing for the EBV. Two patients had the acquired immunodeficiency syndrome (AIDS), and 17 were receiving immunosuppressive therapy for heart or heart-lung transplantation (n = 13), bone marrow transplantation (n = 2), combined variable immune deficiency (n = 1), and vasculitis (n = 1).

RESULTS: Final diagnoses included malignant lymphoma (n = 11), polyclonal lymphoproliferative disorder (n = 7), and hyperplasia of bronchus associated lymphoid tissue (n = 1). The most common CT scan findings consisted of multiple nodules (n = 14), areas of ground glass attenuation (n = 10), septal thickening (n = 6), consolidation (n = 5), lymphadenopathy (n = 5), pleural effusion (n = 5), and solitary endobronchial lesions (n = 2). The nodules measured from 2 mm to 4 cm in diameter, involved mainly the mid and lower lung zones, and frequently had a predominantly peribronchovascular (n = 11) or subpleural (n = 10) distribution.

CONCLUSION: EBV driven lymphoproliferative disorders may range from benign lymphoid hyperplasia to malignant lymphoma. The most common CT findings consist of multiple nodules, frequently located in a predominantly peribronchovascular or subpleural distribution.

Learning Objectives:
1. State the most common CT scan findings seen in patients with EBV driven lymphoproliferative disorders. 2. State five underlying medical conditions leading to development of an EBV driven lymphoproliferative disorder. 3. Describe the pathologic spectrum of lymphoproliferative disorders associated with the EBV. [See also scientific exhibit 0836CH.]

1271 • 3:06 PM
Pulmonary Infections After Bone Marrow Transplantation: Clinical and Radiologic Findings
A.N. Leung, MD, Stanford, CA • M.V. Gosselin, MD • C.H. Napper, MD • S. Brown • W.W. Hu, MD • R.M. Wong • et al
PURPOSE: To assess the clinical and radiologic findings of pulmonary infections diagnosed by invasive means occurring in a consecutive series of 720 adult bone marrow transplant (BMT) recipients during an 8-year period.
MATERIALS AND METHODS: This retrospective study included 55 patients who had a total of 61 pulmonary infections diagnosed via bronchoscopy (n = 44), autopsy (n = 7), percutaneous biopsy (n = 6), open lung biopsy (n = 3), or cutaneous biopsy (n = 1). In each case, the type of transplantation, date of onset of infection, and clinical outcome were obtained by chart review. Chest radiographs (n = 61) and CT scans (n = 17) of the infectious episodes were evaluated by three blinded reviewers.
RESULTS: The 61 infections were caused by fungal (n = 22), viral (n = 22), bacterial (n = 15) and protozoal (n = 2) pathogens. Aspergillosis was the most common fungal infection occurring in 13 allogeneic and 6 autologous recipients with a mean time of onset of 139 days post-BMT. Radiographic findings consisted of areas of consolidation (n = 12) and nodules and/or masses (n = 9). 21 episodes of cytomegalovirus pneumonia occurred in 18 allogeneic and 3 autologous recipients with a mean time of onset of 48 days post-BMT. The most common radiographic finding in CMV pneumonia was increased opacity which ranged from ground-glass (n = 10) to consolidation (n = 8); in 2 patients, the chest radiograph was normal. Pseudomonas pneumonia was the most common bacterial infection occurring in 4 allogeneic recipients; radiographic findings consisted of mass (n = 1), nodules (n = 2), and consolidation (n = 1). 26 of 61 infections (43%) resulted in patient death within 30 days of diagnosis.
CONCLUSIONS: Pulmonary infections are a serious complication of bone marrow transplantation. Aspergillosis and CMV pneumonia are the most common opportunistic infections. Radiographic findings are often nonspecific and in the early stages of viral infection, may be normal.

Learning Objectives:

1272 • 3:15 PM
Anterior Mediastinal Extension of Primary Chest Wall Infections: Role of CT in Detection and Management
E.K. Fishman, MD, Baltimore, MD
PURPOSE: To determine the frequency of mediastinal extension of chest wall infection and the role of CT imaging in detecting and defining its extent for patient triage.
MATERIAL AND METHODS: The CT scans of 20 consecutive patients with infection of the musculature of the chest wall were reviewed. Patients with recent surgery such as medial sternotomy or other chest wall surgical procedure were excluded from the study. Nearly all of the patients were scanned as emergency "add-on" patients from the emergency room where musculoskeletal infection was clinically suspected. 13 of the patients had a documented positive history of intravenous drug abuse. Scans were routinely performed with 100-120 cc of iodinated contrast (Omnipaque-350) injected at 1.5-2.5 cc/sec and with Spiral CT scanning when available. Scan parameters varied but collimation was typically 5mm with images acquired at 5mm intervals.
RESULTS: Of the 20 cases with proven musculoskeletal infection the primary area of involvement was the pectoralis major muscle. Extension to

the sternoclavicular joint was not uncommon with bony erosion of clavicular head and or sternum seen in seven cases. Extension of in to thge anterior mediastinum was definitely present in 5 cases and have been present in 1 additional case although this was never documented by culture or surgical drainage. No cases of pseudoaneurysm vascular occlusion was seen. Cases of mediastinal extension were routinely drained surgically.
CONCLUSION: CT especially spiral CT with rapid infusion has t shown to provide an excellent means for the detection and exten musculoskeletal infection. In the evaluation of the chest wall especially the patient with a history of intravenous drug abuse it is important carefully evaluate the anterior mediastinum for extension of the prim disease process. Detection with CT can lead to early intervention prevent potentially serious complications.

Learning Objectives:
1. Understand the importance of imaging the anterior mediastinum cases of chest wall infection. 2. Understand the role of CT, especially Sp CT in evaluation of chest wall infection. 3. Appreciate the frequency mediastinal extension of chest wall infection and the usual lack of clin suspicion of this process. 4. Identify the role of CT in imaging musculosi etal infection especially in the immunocomprimised pt or IV drug abuse

---

Wednesday Afternoon • Room S505AB

Appendix 3

1273 • 2:30 PM
MR Imaging Lymphography with Superparamagnetic Iron Oxide
L.H. Schwartz, MD, New York, NY • J.A. Koutcher, MD, PhD • C. Matei, BSc • Fisher • S.J. McLachlan, PhD
PURPOSE: To determine if the administration of Combidex (Code 7227) superparamagnetic iron oxide contrast agent, will discriminate tumor fro inflammatory lymphadenopathy and to determine the effect on contrast various pulse sequence parameters.
METHOD AND MATERIALS: 25 Fischer rat hind paws were treated with mammary carcinoma tumor model, R3230AC, and were imaged at 1.5 before and after IV Combidex administration. Nine additional Fischer rat were injected with Freund's adjuvant to induce an inflammatory response in popliteal lymph nodes. Conventional spin echo (CSE) (2000/20,80), fas: spin echo (FSE-T2 and FSE-PD) (4000/105 and 4000/16 with ETL's o: 8,16,32), and gradient echo images were acquired. Contrast to noise ratios (CNR) relative to muscle were calculated and histopathologic correlation was obtained for all lymph nodes.
FINDINGS: Histopathologic analysis revealed tumor in 23 of 25 rat lymph nodes treated with the mammary carcinoma model. The mean change in CNR for the inflammatory lymph nodes for the FSE-T2 sequence were -40.1%, -47.3% and -43.2% with ETL's of 8, 16 and 32, respectively, and 3.7%, 6.1% and -9.2% for the tumor-bearing nodes. The mean change in contrast for the inflammatory nodes for the FSE-PD sequence were -59.1%, -55.5%, and -53.85% with ETL's of 8, 16 and 32 respectively and -65.2%, 28.8% and 37.8% for tumor bearing nodes (not significant). The greatest changes in CNR were seen with the gradient echo sequence (79± 0.4%). No statistically significant differences between inflammatory and tumor-bearing lymph nodes were seen with the CSE and gradient echo sequences. Changes in ETL did not significantly alter the CNR for either the inflammatory or tumor-bearing nodes.
CONCLUSION: The greatest difference in CNR loss between inflammatory and neoplastic lymph nodes were seen on the fast spin echo pulse sequence. ETL did not affect CNR. Both inflammatory and tumor-bearing lymph nodes showed CNR loss with the other pulse sequences

Learning Objectives:
1. The ability to distinguish inflammatory from neoplastic lymph nodes is aided with Combidex.
2. Pulse sequence parameters greatly affect the contrast to noise and the ability to discriminate between types of lymphadenopathy.

1274 • 2:39 PM
A Modular Lymphographic MR Imaging Contrast Agent for Lymph Node Enhancement and DNA Transfection
E.R. Wisner, DVM, Columbus, OH • M.H. Nantz, PhD
PURPOSE: To develop an agent for indirect MR lymphography with potential for regional gene transfection therapy.
MATERIALS AND METHODS: A gadolinium chelated liposomal contrast agent was prepared and MR imaging efficacy was examined by indirect magnetic resonance lymphography. A lipidic N,N'-dimethylethylenediamine derivative containing a 10,12-diyne-diacyl domain was treated with

exposure, but did demonstrate Bcl-x$_L$ phosphorylation in the presence of other tubulin targeting agents. As observed for Bcl-2, phosphorylation of Bcl-x$_L$ was accompanied by phosphorylation of Raf-1. Phosphorylation of these three proteins failed to occur or was much less pronounced when cells grown at high density were challenged with drug. Reduced Raf-1 expression, observed after treatment of cells with geldanamycin prior to and during incubation with the MT-active drugs, accompanied the diminished phosphorylation of Bcl-x$_L$. Taken together, these results suggest that Bcl-x$_L$, like Bcl-2, is phosphorylated following disruption of MT architecture. By analogy with Bcl-2, this phosphorylation may play a critical role in modulating Bcl-x$_L$ function, and could be an important determinant of MT-directed chemotherapeutic efficacy in human tumors.

#1303 Like p53, the proliferation-associated protein p120 accumulates in human cancer cells following exposure to anticancer drugs. Blagosklonny, M.V., Iglesias, A., Zhan, Z., Fojo, T. Medicine Branch, NCI, NIH, Bethesda, MD 20892

Accumulation of wild-type (wt) p53 protein following DNA damage is a cellular response to preserve genomic integrity. This accumulation is independent of transcription; in turn, p53 transcriptionally induces other factors. Herein we demonstrate that p120, a proliferation-associated protein, was induced by microtubule-active and DNA-damaging drugs in human cancer cells. Induction of p120 was independent of p53; and expression of exogenous wt p53 induced p21$^{WAF1/CIP1}$ but not p120, excluding p120 as a transcriptional target of p53. Like p53, induction of p120 by anticancer drugs did not require transcription. Induction of p120 by actinomycin-D and other DNA-damaging drugs could be demonstrated at concentrations that inhibit RNA synthesis and p120 mRNA levels. Inhibition of proteasomes resulted in accumulation of higher molecular weight proteins, reacting with anti-p120 antibodies. While these observations suggest that the mechanisms of p120 and p53 induction are similar and involve inhibition of degradation, the stimuli for induction were not identical. Microtubule active DNA that dient fol-

Appendix 4

#1304 In vivo metabolic and tumor growth delay studies with paclitaxel and bryostatin 1, a PKC inhibitor, are sequence dependent. J.A. Koutcher, C. Matei, K. Zakian, D. Ballon and G.K. Schwartz. Memorial Sloan Kettering Cancer Ctr, New York, NY.

We undertook this study to determine if Bryostatin 1 enhances response to paclitaxel, and if there is a sequence dependence to this effect in vivo. The effect of paclitaxel and multiple dose levels of Bryostatin 1 on tumor metabolism and survival was investigated. Tumor doubling times (TDT) were evaluated for mice treated with single agent Bryostatin 1, paclitaxel, and the combinations of Bryostatin 1 → paclitaxel and paclitaxel→Bryostatin 1, in vivo, using a murine mammary carcinoma tumor model. The maximum tolerated single dose (LD10) of Bryostatin 1 was 80 ug/kg. This dose induced a tumor doubling time of 4.2 ± 0.3 days (n = 10) compared to 2.9 ± 0.3 days for untreated mice (n = 10) (p < 0.01). Metabolic studies at doses of 160, 120, 80 and 60 ug/kg showed that at 12–24 hours post treatment, tumors were acidic ($\Delta pH = 0.18 \pm 0.02$ (80 ug/kg)) and energy depletion was observed by 31P NMR spectroscopy. Based on these data, the effect of combining Bryostatin 1 with paclitaxel on tumor growth was evaluated. Paclitaxel was administered at a dose of 30 mg/kg i.v. × 3 doses each separated by 12 hours. The interval between Bryostatin 1 → paclitaxel and paclitaxel → Bryostatin 1 was 12 hours. Tumor bearing mice received 3 cycles of chemotherapy, each separated by one week. Tumor doubling times were 23.4 ± 1.7 days (paclitaxel), 9.3 ± 1.9 (Bryostatin 1 → paclitaxel), and 30.0 ± 0.9 days (paclitaxel → Bryostatin 1). The differences between paclitaxel, paclitaxel → Bryostatin 1, and Bryostatin 1 → paclitaxel were all significant (p < 0.01). These data indicate that Bryostatin can actually have inhibitory effects on the efficacy of paclitaxel, and emphasize that the interaction of Bryostatin 1 and paclitaxel are sequence dependent as suggested by previous in vitro data, indicating the importance of drug sequence in future clinical trials of this agent.

#1305 Loss of p53 function precedes tubulin mutations in the development of paclitaxel (PTX) resistance. Giannakakou, P., Blagosklonny, M.V., and Fojo, T. Medicine Branch, DCS, NCI, NIH, Bethesda, MD 20892.

We examined the p53 status of 3 PTX resistant human ovarian carcinoma sublines, isolated from A2780 cells by stepwise increases in PTX concentration from 5–15 ng/ml. The sublines growing in 15 ng/ml PTX exhibit a non-MDR1 resistant phenotype due to acquired tubulin mutations which impair PTX's interaction with tubulin. In contrast to parental cells, all three PTX resistant sublines exhibit high levels of transcriptionally inactive p53 protein, unresponsive to DNA damaging agents. Sequencing of p53 revealed in each cell line a distinct point mutation in the DNA binding domain. Infection with an adenovirus expressing wt p53 resulted in induction of p21 demonstrating an intact p53 pathway. However, restoration of wt p53 in the PTX resistant sublines did not affect cellular sensitivity to PTX, although it increased sensitivity to adriamycin. To further probe the role of p53 in the development of PTX resistance, we examined the p53 status in early isolates growing in 5 ng/ml PTX. Two of the three sublines had mutant p53s that were transcriptionally inactive; while the third subline had a nonfunctional wt p53,

with undetectable/uninducible protein secondary to a marked reduction in p53 mRNA expression. Thus p53 inactivation by either acquired mutations or reduced expression occurs early in the development of PTX resistance. The lack of a functional p53 in all sublines early in the isolation suggests this has a selective advantage. Since PTX sensitivity is not affected by re-introduction of wt p53, it suggests that loss of functional p53 while not directly conferring PTX resistance, facilitates its development.

#1306 Identification of the signaling pathway and the biological effect of paclitaxel-dependent transcriptional activation of IL-8 expression in human ovarian and lung cancer. Lee, L.F., Collins, T.S., and Ting, J.P. Department of Biology, Department of Surgery, Department of Microbiology and Immunology; Lineberger Comprehensive Cancer Center, University of North Carolina at Chapel Hill, NC 27599-7295.

The primary mechanism of action of paclitaxel is attributed to its ability to bind microtubules, however, its efficacy exceeds that of conventional microtubule-disrupting agents, suggesting that it may have additional cellular effects. Previously, we demonstrated that paclitaxel can induce IL-8 gene transcription in subsets of human ovarian cancer lines. Recent studies have extended this observation to lung cancer. The induction in ovarian cancer does not appear to be linked to the LPS (lipopolysaccharide) pathway of IL-8 gene induction. We have also identified the AP-1 and NF-κB binding sites in the IL-8 promoter that are required for activation by paclitaxel in responsive cells. Supershift experiments demonstrated that the AP-1 component contains c-Jun. Since JNK/SAPK (c-Jun NH2 terminal kinase/stress activated protein kinase) is required for phosphorylation and activation of c-Jun, we also determined that JNK is activated by paclitaxel. To study the biologic effect of IL-8 on tumor growth, the human IL-8 gene was transfected into IL-8 non-producing human ovarian cancer cell lines. The production of hu-IL-8 dramatically suppressed tumor growth in nude mice. Histologic analysis of the site of injection showed marked infiltration of immune cells. These results suggest that IL-8 induction by tumor cells may be beneficial to the host by attracting immune cells to the tumor site.

#1307 Evidence of taxol-induced apoptotic cell death via a signaling pathway independent of cell cycle arrest. Fan, W., Huang, Y., Miller, M.C., Norris, J.N. and Willingham, M.C. Medical University of South Carolina, Charleston, SC 29425

Taxol has shown significant cell-killing activity in a number of solid tumor cells through induction of apoptosis, but it is unclear whether this finding suggests a novel mechanism of action for taxol against tumor cells or just represents an end product of taxol's well-known effects on microtubules and cell cycle arrest. Our recent studies demonstrated that pretreatment of tumor cells with glucocorticoids could significantly inhibit taxol's cell-killing activity but not mitotic arrest, suggesting that taxol-induced apoptosis might occur via a signaling pathway independent of mitotic arrest (Cell. Pharmacol. 3:343–348 and 3:435–440, 1996). We have now obtained more evidence supporting this hypothesized pathway. 1) apoptotic cell death was triggered as long as the cells were exposed to taxol for 1 hr, this phenomenon clearly contrasts with the reversible manner of taxol binding to microtubules; 2) By utilizing baccatin III, a precursor of taxol, apoptotic cell death was clearly observed in the cells without a G2/M arrest; 3) the I-κB/NF-κB signaling pathway was found to mediate the inhibitory action of glucocorticoids on taxol-induced apoptosis. All these results support that taxol-induced apoptosis is via a pathway independent of cell cycle arrest. (Supported by NIH CA71581 and CA58846).

#1308 Genetic susceptibility to microtubule-active cancer chemotherapeutic drugs: p53 action and the role of microtubule associated protein 4 (MAP4). Zhang, C., Yang, J.M., White, E., Murphy, M., Levine, A.J., and Hait, W.N. UMDNJ/Robert Wood Johnson Medical School, The Cancer Institute of New Jersey, New Brunswick, NJ 08901, Rutgers University, Piscataway, NJ 08854, and Princeton University, Princeton, NJ 08544.

p53 mutations decrease the sensitivity to vinca alkaloids (VA) and increase the sensitivity to paclitaxel (TAX). MAP4, which regulates the polymerization of microtubules, is controlled by the transcriptional activity of p53. Therefore, we studied whether MAP4 expression accounts for the p53-dependent changes in sensitivity to antimitotic drugs. BRK cells transfected with a temperature-sensitive mutant of p53 (tsp53Val^{135}) expressed 5–7 fold more MAP4 at the restrictive temperature (p53 mt) and were 9-fold more sensitive to TAX and 4-fold more resistant to VA. A31 cells transfected with MAP4 were 10-fold (IC$_{50}$ = 200 nM) more sensitive to TAX and 10-fold (IC$_{50}$ = 1 μM) more resistant to VA than vector-transfected controls. This was associated with marked changes in drug-induced apoptosis and cell-cycle distribution. Immunofluorescence microscopy revealed that overexpression of MAP4 increased polymerization of microtubules and cellular TAX-binding. UV-irradiation of C127 breast cancer cells increases endogenous wt p53 and produced a 5-fold decrease in MAP4 levels at 24 hours, which was associated with decreased sensitivity to TAX and increased sensitivity to vinblastine. At 48 hours, when p53 and MAP4 returned to baseline, the changes in sensitivity was no longer observed. Since MAP4 stabilizes polymerized microtubules, overexpression of this gene provides a plausible mechanism to explain the sensitivity to microtubule-active drugs in the presence of mutant p53 and may be used to design more rational combination therapies.